bioRxiv preprint doi: https://doi.org/10.1101/2020.08.07.238766; this version posted August 7, 2020. The copyright holder for this preprint (which was not certified by peer review) is the author/funder, who has granted bioRxiv a license to display the preprint in perpetuity. It is made available under aCC-BY-NC-ND 4.0 International license.

The Pancreatic Tumor Microenvironment Buffers Redox Imbalance Imposed by Disrupted Mitochondrial Metabolism

Samuel A. Kerk[1,2], Lin Lin[2], Amy L. Myers[2], Brandon Chen[2], Peter Sajjakulnukit[1,2], Anthony Robinson[3], Galloway Thurston[2], Barbara S. Nelson[1,2], Samantha B. Kemp[4], Nina G. Steele[3], Megan T. Hoffman[2], Hui-Ju Wen[2], Daniel Long[2], Sarah E. Ackenhusen[5], Johanna Ramos[2], Xiaohua Gao[2], Li Zhang[2], Anthony Andren[2], Zeribe C. Nwosu[2,6], Stefanie Galbán[1,7,10], Christopher J. Halbrook[2], David B. Lombard[1,9], Haoqiang Ying[11], Howard C. Crawford[1,2,10], Marina Pasca di Magliano[1,6,10] †Yatrik M. Shah[1,2,8,10], †Costas A. Lyssiotis[1,2,8,10]

[1]Doctoral Program in Cancer Biology, University of Michigan, Ann Arbor, MI 48109
[2]Department of Molecular & Integrative Physiology, University of Michigan, Ann Arbor, MI 48109
[3]Department of Cell & Developmental Biology, University of Michigan, Ann Arbor, MI 48109
[4]Molecular and Cellular Pathology Graduate Program, University of Michigan, Ann Arbor, MI 48109
[5]Program in Chemical Biology, University of Michigan, Ann Arbor, MI 48109
[6]Department of Surgery, University of Michigan, Ann Arbor, MI 48109
[7]Department of Radiology, University of Michigan, Ann Arbor, MI 48109
[8]Department of Internal Medicine, Division of Gastroenterology and Hepatology, University of Michigan, Ann Arbor, MI 48109
[9]Department of Pathology and Institute of Gerontology, University of Michigan, Ann Arbor, MI 48109
[10]Rogel Cancer Center, University of Michigan, Ann Arbor, MI 48109
[11]Department of Molecular and Cellular Oncology, University of Texas MD Anderson Cancer Center, Houston, TX 77054

†Correspondence: clyssiot@med.umich.edu, shahy@med.umich.edu

ABSTRACT

The tumor microenvironment (TME) in pancreatic ductal adenocarcinoma (PDA) restricts vascularization and consequently nutrient and oxygen access and drug delivery. Concurrently, recent work also demonstrates that the TME directly provides metabolites that facilitate cancer cell survival, growth, and therapeutic resistance. Redox imbalance is another restraint on cellular proliferation, yet it is unknow how the TME contributes to the maintenance redox homeostasis in PDA cells. Here, we demonstrate that the loss of mitochondrial glutamate-oxaloacetate transaminase 2 (GOT2), a component in the malate-aspartate shuttle (MAS), disturbs redox homeostasis and halts proliferation of PDA cells in vitro. Surprisingly, we found GOT2 knockdown has no effect on in vivo tumor growth. We demonstrate that this discrepancy is explained by heterocellular pyruvate exchange from the TME, including from cancer associated fibroblasts (CAF). More broadly, pyruvate similarly confers resistance to inhibitors of mitochondrial respiration. Blocking pyruvate uptake through genetic or pharmacologic inhibition of monocarboxylate transporter 1 (MCT1) abrogated pyruvate-mediated restoration of redox homeostasis. In sum, this work describes a potential resistance mechanism mediated by metabolic crosstalk within the pancreatic TME. These findings have important implications for metabolic treatment strategies since several mitochondrial inhibitors are currently in clinical trials for PDA and other cancers.

INTRODUCTION

Cancer cells depend on deregulated metabolic programs to meet their energetic and biosynthetic demands[1,2]. Metabolic therapies aim to preferentially target these dependencies[3]. This approach has shown promise in preclinical models of pancreatic ductal adenocarcinoma (PDA) – one of the deadliest major cancers, notoriously resistant to other modern anti-cancer therapies[4,5]. Pancreatic tumors are poorly vascularized and nutrient austere[6]. Therefore, cancer

bioRxiv preprint doi: https://doi.org/10.1101/2020.08.07.238766; this version posted August 7, 2020. The copyright holder for this preprint (which was not certified by peer review) is the author/funder, who has granted bioRxiv a license to display the preprint in perpetuity. It is made available under aCC-BY-NC-ND 4.0 International license.

cells commandeer metabolic pathways to scavenge and utilize nutrients[5]. A wealth of recent literature has identified this is mediated predominantly by mutant KRAS (KRAS*), the oncogenic driver in most pancreatic tumors[7-12]. KRAS* has also been implicated in shaping the pancreatic tumor microenvironment[13]. PDA tumors exhibit a complex tumor microenvironment[14,15] with metabolic interactions between malignant and non-malignant parenchymal cells enabling and facilitating tumor progression[16]. Since KRAS* has proven to be difficult to target directly, disrupting downstream metabolic crosstalk mechanisms in PDA is a compelling alternative approach[17].

In support of this idea, previous work from our lab described that PDA cells are uniquely dependent on KRAS*-mediated rewiring of glutamine metabolism for protection against oxidative stress[9]. Mitochondrial glutamate oxaloacetate transaminase 2 (GOT2) is critical for this rewired metabolism. In normal physiology, GOT2 functions in the malate-aspartate shuttle (MAS), a mechanism by which cells transfer reducing equivalents between the cytosol and mitochondria to balance the two independent NADH pools and maintain redox balance (**Fig.1A**). PDA cells driven by KRAS* divert metabolites from the MAS and increase flux through malic enzyme 1 (ME1) to produce NADPH[9]. Since this pathway is critical for PDA, we set out to evaluate GOT2 as a potential therapeutic target. This led to the observation that GOT2 was required for in vitro but not in vivo tumor growth. Ultimately, through metabolomics analyses and manipulation of the redox state in PDA cells, we discovered that pancreatic cancer-associated fibroblasts (CAFs) release pyruvate, which can be consumed by PDA cells to alleviate the redox imbalance induced by impaired mitochondrial metabolism. These data emphasize an under-appreciated role for GOT2 in pancreatic tumor redox homeostasis, and, perhaps more importantly, reinforce that the tumor microenvironment plays a major role in cancer metabolism and therapeutic resistance.

RESULTS

GOT2 is required for PDA colony formation in vitro

To expand on our previous work studying GOT2 in PDA[9], and to evaluate GOT2 as a potential therapeutic target, we generated a panel of PDA cell lines with doxycycline-inducible expression of either a control non-targeting shRNA (shNT) or two independent shRNAs (sh1, sh2) targeting the GOT2 transcript. Cells cultured in media containing doxycycline (+DOX) exhibited a marked decrease in GOT2 protein expression compared to cells cultured in media without doxycycline (-DOX) (**Fig.1B; Extended Data Fig.1A**). This knockdown was specific for GOT2, relative to the cytosolic aspartate aminotransaminase GOT1 (**Extended Data Fig.1D**). Having validated GOT2 knockdown, we tested the importance of GOT2 for cellular proliferation. In general, GOT2 knockdown in PDA cells impaired colony formation (**Fig.1C,D; Extended Data Fig.1B,C**). Consistent with our previous report[9], GOT2 was not required for the proliferation of non-transformed pancreatic cell types (**Extended Data Fig.1E,F).**

Since GOT2 has several vital metabolic roles in a cell (**Fig.1A**), the changes caused by decreased GOT2 expression in PDA cells were examined using liquid chromatography coupled tandem mass spectroscopy (LC-MS/MS). Numerous changes in the intracellular metabolome of GOT2 knockdown cells were observed (**Fig.1E,F; Extended Data Fig.1G,H**). Of note, the products of the GOT2-catalyzed reaction, aspartate (Asp) and α-ketoglutarate (αKG), were decreased (**Fig.1G**). In addition to reduced αKG, there was a decrease in most TCA cycle intermediates (**Fig.1H**). These data demonstrate that loss of GOT2 in vitro depletes Asp and

bioRxiv preprint doi: https://doi.org/10.1101/2020.08.07.238766; this version posted August 7, 2020. The copyright holder for this preprint (which was not certified by peer review) is the author/funder, who has granted bioRxiv a license to display the preprint in perpetuity. It is made available under aCC-BY-NC-ND 4.0 International license.

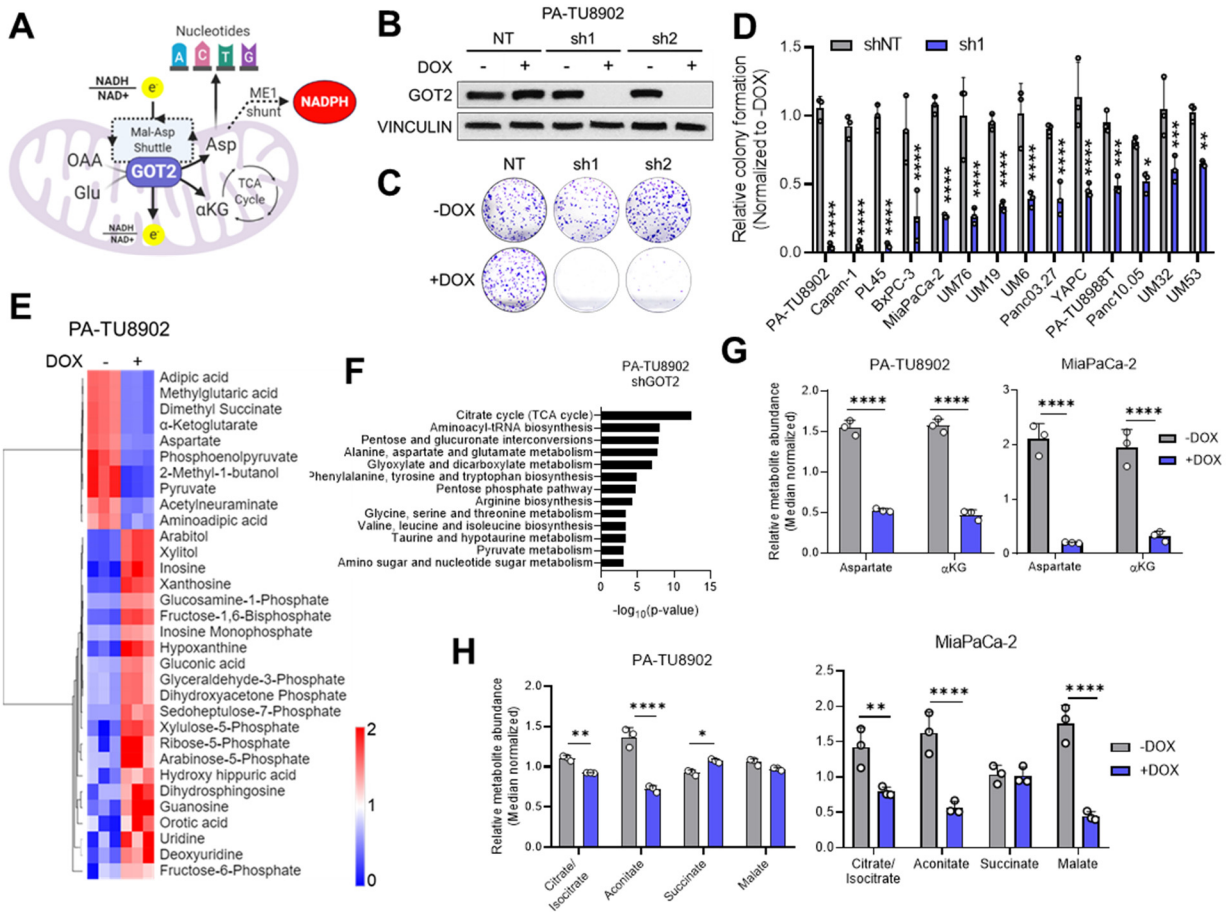

Fig.1 GOT2 knockdown impairs in vitro PDA colony formation. A) Schematic depicting the metabolic roles of GOT2 in PDA. **B)** Western blot of GOT2 expression with Vinculin loading control in PA-TU8902 cells expressing doxycycline-inducible shNT or two independent shRNA sequences against GOT2. **C)** Images of representative wells showing PA-TU8902 colony formation after GOT2 knockdown. **D)** Relative colony formation after GOT2 knockdown with sh1 across a panel of PDA cell lines. **E-H)** Metabolites significantly changed between +DOX (n=3) and –DOX (n=3) ($p<0.05$, $-1>\log2FC>1$) after GOT2 knockdown as assessed by metabolomics. **E)** Heatmap depicting changes in relative metabolite abundances in PA-TU8902 cells with 2D unsupervised hierarchical clustering. **F)** Metabolic pathways significantly changed in PA-TU8902 cells, as determined via Metaboanalyst. **G)** Relative abundances of Aspartate and αKG in PA-TU8902 and MiaPaCa-2 cells. **H)** Relative abundances of TCA cycle intermediates in PA-TU8902 and MiaPaCa-2 cells. Bars represent mean ± SD, *$p<0.05$, **$p<0.01$, ***$p<0.001$, ****$p<0.0001$.

αKG, and also induces a strong growth inhibitory phenotype in vitro, prompting further exploration of GOT2 as a metabolic target in PDA in vivo.

GOT2 is not required for PDA tumor growth in vivo

PDA cell lines were injected subcutaneously into the flanks of immunocompromised (NOD Scid gamma; NSG) mice and tumors were allowed to establish for 7 days. Mice were then fed normal chow or doxycycline chow ad libitum. Surprisingly, despite the inhibitory in vitro phenotype and robust suppression of GOT2 expression in vivo, tumors from five different cell lines grew unimpeded with GOT2 knockdown (**Fig.2A-C; Extended Data Fig.2A,B**). Tissue slices from

bioRxiv preprint doi: https://doi.org/10.1101/2020.08.07.238766; this version posted August 7, 2020. The copyright holder for this preprint (which was not certified by peer review) is the author/funder, who has granted bioRxiv a license to display the preprint in perpetuity. It is made available under aCC-BY-NC-ND 4.0 International license.

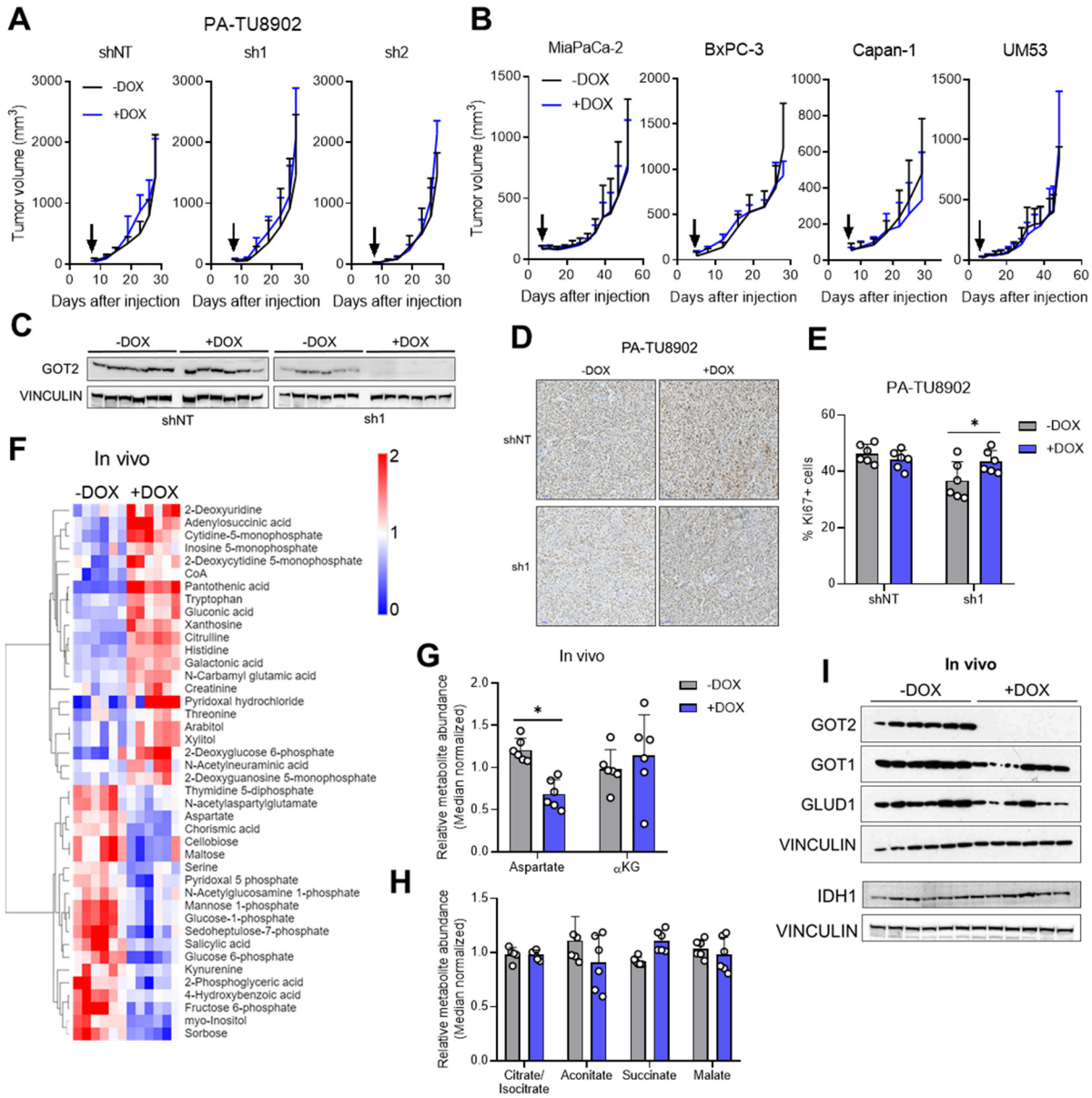

Fig.2 GOT2 is not required for PDA tumor growth in vivo. A) Growth of PA-TU8902 GOT2 knockdown subcutaneous PDA tumors in NSG mice (n=6 tumors per group). Arrows indicate administration of doxycycline chow. **B)** Growth across a panel of subcutaneous PDA GOT2 sh1 knockdown tumors in NSG mice (n=6 tumors per group). Arrows indicate administration of doxycycline chow. **C)** Western blot for expression of GOT2 and Vinculin loading control in PA-TU8902 GOT2 knockdown subcutaneous tumors. **D)** Representative images of Ki67 staining in tissue slices from PA-TU8902 GOT2 knockdown tumors. **E)** Quantification of nuclei positive for Ki67 in tissue slices from (B) (n=6 tumors per group). **F-H)** Metabolites significantly changed between PA-TU8902 GOT2 knockdown +DOX (n=6) and –DOX (n=6) ($p<0.05$, $-0.5>\log2FC>0.5$) subcutaneous tumors. **F)** Heatmap depicting changes in relative metabolite abundances with 2D unsupervised hierarchical clustering. **G)** Relative abundances of Aspartate and αKG. **H)** Relative abundances of TCA cycle intermediates. **I)** Western blots for expression of GOT1, GOT2, GLUD1, and IDH1, Vinculin loading control in PA-TU8902 GOT2 knockdown tumors. Bars represent mean ± SD, *$p<0.05$, **$p<0.01$, ***$p<0.001$, ****$p<0.0001$.

these tumors stained for nuclear Ki67 confirmed that tumors lacking GOT2 were proliferative,

bioRxiv preprint doi: https://doi.org/10.1101/2020.08.07.238766; this version posted August 7, 2020. The copyright holder for this preprint (which was not certified by peer review) is the author/funder, who has granted bioRxiv a license to display the preprint in perpetuity. It is made available under aCC-BY-NC-ND 4.0 International license.

and actually displayed a modest, but significant, increase in Ki67-positive nuclei (**Fig.2D,E**). To further examine the role of GOT2 in a more physiologically relevant tumor model, PDA cells were injected orthotopically into the pancreas of NSG mice and tumors were allowed to establish for 7 days before feeding the mice regular or doxycycline chow. Similar to the subcutaneous model, GOT2 knockdown had no effect on the growth of orthotopic tumors (**Extended Data Fig.2C**).

Having observed a discrepancy between in vitro and in vivo dependence on GOT2 for proliferation, the relative abundances of intracellular metabolites from subcutaneous tumors were analyzed via LC-MS/MS to compare the metabolic changes between cell lines and tumors following loss of GOT2. While GOT2 knockdown induced some changes in tumor metabolite levels, the affected metabolic pathways were distinct from those observed in vitro (**Fig.2F; Extended Data Fig.2D**). Asp abundance was significantly decreased, yet αKG levels remained constant (**Fig.2G**), and TCA cycle intermediates were unaffected (**Fig.2H**). This led us to initially hypothesize that PDA cells rewire their metabolism in vivo to maintain αKG levels when GOT2 is knocked down. However, upon examination of the expression of other αKG-producing enzymes in GOT2 knockdown tumors, we did not observe a compensatory increase in expression (**Fig.2I**). Certainly, expression does not always dictate metabolic flux, but these data led us to adopt an alternative, cell-extrinsic hypothesis to explain the different in vitro and in vivo GOT2 knockdown phenotypes.

Cancer-associated fibroblast conditioned media supports colony formation in GOT2 knockdown cells in vitro

Human PDA tumors develop a complex microenvironment composed of a tumor-promoting immune compartment, a robust fibrotic response consisting of diverse stromal cell types, and a dense extracellular matrix (ECM)[15]. Additionally, we and others have previously reported mechanisms by which CAFs in the stroma engage in cooperative metabolic crosstalk with pancreatic cancer cells[18-20]. So, we hypothesized that CAFs were supporting PDA metabolism following GOT2 knockdown. First, while the subcutaneous tumor milieu in immunocompromised mice is less complex than that of a human PDA tumor, α-smooth muscle actin (αSMA) staining revealed that activated fibroblasts comprised a substantial portion of the microenvironment in tumors regardless of GOT2 status (**Extended Data Fig.3A**). To investigate potential metabolic crosstalk in a simplified setting, PDA cells were cultured in vitro with conditioned media (CM) from human CAFs. In support of our hypothesis, CAF CM promoted colony formation in PDA cells with GOT2 knockdown in a dose-dependent manner (**Fig.3A,B; Extended Data Fig.3B**). Furthermore, CAF CM displayed a more pronounced rescue phenotype compared to CM from tumor-educated macrophages (TEMs) or from PDA cells (**Extended Data Fig.3D**).

To begin to identify the factors in CAF CM responsible for this effect, CAF CM was boiled, filtered through a 3 kDa cut-off membrane, or subjected to cycles of freezing and thawing. In each of these conditions, CAF CAM supported colony formation in GOT2 knockdown cells, suggesting the relevant factor(s) was a metabolite (**Fig.3C; Extended Data Fig.3C**). The relative abundances of metabolites in CAF CM determined via LC-MS/MS demonstrated that pyruvate was one of the most abundant metabolites released by CAFs into the conditioned media, at a concentration near 250 μM (**Fig.3D,E; Extended Data Fig.3E**). Consistent with the idea of metabolite exchange, CAF-derived pyruvate was taken up by PDA cells, as cells cultured in CAF CM had elevated levels of intracellular pyruvate (**Fig.3F**).

bioRxiv preprint doi: https://doi.org/10.1101/2020.08.07.238766; this version posted August 7, 2020. The copyright holder for this preprint (which was not certified by peer review) is the author/funder, who has granted bioRxiv a license to display the preprint in perpetuity. It is made available under aCC-BY-NC-ND 4.0 International license.

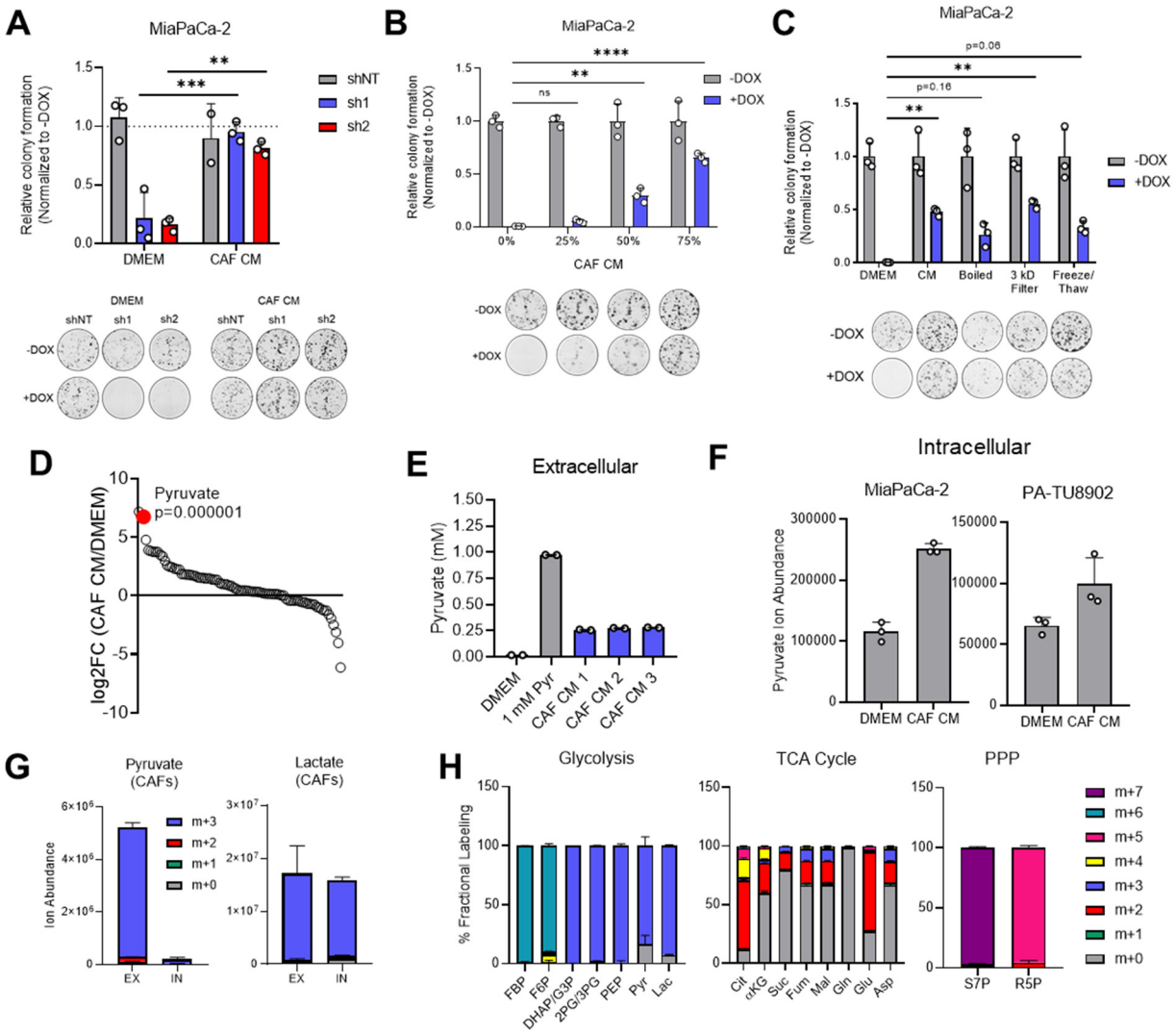

Fig.3 CAF CM restores PDA colony formation after GOT2 knockdown in vitro. A) Relative colony formation of MiaPaCa-2 GOT2 knockdown cells cultured in DMEM or CAF CM, with images of representative wells. **B)** Relative colony formation of MiaPaCa-2 GOT2 knockdown cells cultured in different doses of CAF CM, with images of representative wells. **C)** Relative colony formation of MiaPaCa-2 knockdown cells cultured in DMEM or fresh CAF CM, boiled CM, CM passed through a 3 kD filter, or CM subjected to freeze/thaw cycles, with images of representative wells. **D)** Abundance of metabolites in CAF CM compared to DMEM ranked according to log2FC. **E)** Quantification of pyruvate in three independent CAF CM batches along with a 1 mM pyruvate control spiked into DMEM. **F)** Relative intracellular abundance of pyruvate in PDA cells cultured in DMEM or CAF CM. **G)** Ion abundance of pyruvate and lactate isotopologues in intra and extracellular fractions from CAFs cultured in 13C-Glucose. **H)** Fractional labelling of intracellular isotopologues in glycolysis, TCA cycle, and the pentose phosphate pathway (PPP) from CAFs cultured with U13C-Glucose. Bars represent mean ± SD, *p<0.05, **p<0.01, ***p<0.001, ****p<0.0001. Fructose-6-phosphate (F6P), fructose-1,6-bisphosphate (FBP), dihydroxyacetone phosphate (DHAP), glyceraldehyde-3-phosphate (G3P), 2-phosphoglycerate (2PG), phosphoenol pyruvate (PEP), pyruvate (Pyr), lactate (Lac), citrate (Cit), succinate (Suc), fumarate (Fum), malate (Mal), glutamine (Gln), glutamate (Glu), sedoheptulose-7-phosphate (S7P), ribose-5-phosphate (R5P).

bioRxiv preprint doi: https://doi.org/10.1101/2020.08.07.238766; this version posted August 7, 2020. The copyright holder for this preprint (which was not certified by peer review) is the author/funder, who has granted bioRxiv a license to display the preprint in perpetuity. It is made available under aCC-BY-NC-ND 4.0 International license.

To better understand the production and release of pyruvate in CAFs, an isotope tracing experiment on CAFs with uniformly labeled (U13C)-Glucose was performed. The pyruvate released by CAFs was indeed produced from glucose (**Fig.3G**), and, in support of previous studies[21,22], these CAFs displayed labelling patterns indicative of glycolytic metabolism (**Fig.3H**).

Pyruvate compensates for GOT2 knockdown in vitro

To determine whether pyruvate was the metabolite responsible for the rescue of GOT2 knockdown, cells were cultured in media supplemented with extracellular pyruvate. In a dose-dependent fashion, pyruvate increased colony formation in GOT2 knockdown cells (**Fig.4A,B**). This rescue was observed at both supra-physiological levels of pyruvate (1 mM) and at the levels we reported in CAF CM (250 μM). Furthermore, the concentration of pyruvate in mouse serum was previously reported to be 250 μM[23], indicating that subcutaneous tumors are exposed to a dose of pyruvate that is able to rescue growth during GOT2 knockdown. Additionally, PDA cells expressing a genetically-encoded, fluorescent ATP sensor indicated that ATP levels dropped with GOT2 knockdown, and were restored with pyruvate supplementation (**Fig.4C**), reflecting the link between TCA cycle activity, respiration, and oxidative phosphorylation. The increase in ATP levels also correlated with an increase in overall proliferation (**Extended Data Fig.4A**). Furthermore, having identified a metabolite that permits in vitro proliferation of PDA cells without GOT2, CRISPR-Cas9 GOT2 knock out (KO) cells were engineered (**Extended Data Fig.4B**). In support of the data generated using the doxycycline-inducible shRNA, GOT2 KO impaired colony formation of PDA cells, which was similarly restored through extracellular pyruvate supplementation (**Fig.4D; Extended Data Fig.4C**).

In addition to pyruvate, both Asp and αKG were present in CAF CM (**Extended Data Fig.3E**). Previous studies have illustrated that aspartate is rate limiting for proliferation[24-30]. Given that GOT2 is the predominant source of aspartate in PDA cells (**Fig.1A**), we also tested if aspartate, αKG, or the combination could rescue GOT2. While the combination afforded rescue, this required supraphysiological concentrations (4mM αKG, 10mM Asp). Interestingly, while rescue of GOT2 knockdown could be achieved with both Asp and αKG, pyruvate promoted GOT2 knockdown to an even greater degree than this combination (**Extended Data Fig.4F**). Considering that lack of rescue with single agent Asp could be explained by inefficient import by PDA cells, as has been reported[30], we confirmed that PDA cells cultured with 10mM Asp displayed elevated levels of intracellular aspartate (**Extended Data Fig.4D,E**). Furthermore, providing cells with purine or pyrimidine nucleobases, metabolites downstream of Asp and responsible for proliferation (**Fig.1A**)[31], did not restore colony formation after GOT2 knockdown (**Extended Data Fig.4G**). As such, these data demonstrate while Asp and αKG can rescue GOT2 knockdown, several lines of evidence conclude that this is not the mechanism imparted by CAF CM.

Pyruvate is a pleiotropic molecule and has numerous fates and functions. These include roles in redox and nitrogen balance and as a fuel for myriad biosynthetic precursors and pathways[32]. Thus, we next set forth to determine the mechanism(s) by which pyruvate afforded rescue of GOT2 knockdown or KO.

First, the potential for pyruvate to fuel mitochondrial metabolism was evaluated. As discussed above, GOT2 knockdown disrupted the TCA cycle, likely resulting from a decrease in αKG.

bioRxiv preprint doi: https://doi.org/10.1101/2020.08.07.238766; this version posted August 7, 2020. The copyright holder for this preprint (which was not certified by peer review) is the author/funder, who has granted bioRxiv a license to display the preprint in perpetuity. It is made available under aCC-BY-NC-ND 4.0 International license.

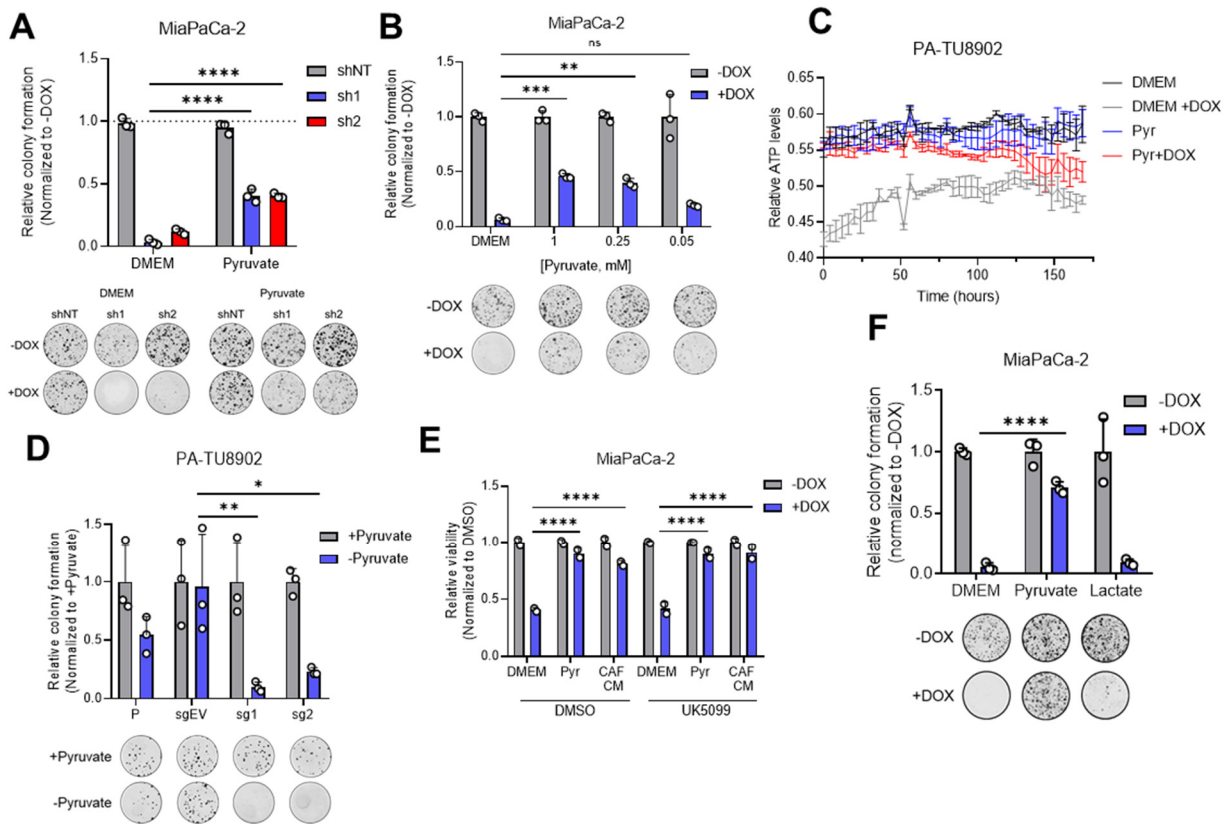

Fig.4 Pyruvate compensates for GOT2 knockdown in vitro. A) Relative colony formation of MiaPaCa-2 GOT2 knockdown cells cultured in DMEM or 1 mM pyruvate, with images of representative wells. **B)** Relative colony formation of MiaPaCa-2 knockdown cells cultured in DMEM or the indicated doses of pyruvate, with images of representative wells. **C)** Relative ATP levels over time in PA-TU8902 GOT2 knockdown cells cultured in DMEM or 1 mM pyruvate. **D)** Relative colony formation of PA-TU8902 GOT2 knockout cells cultured in DMEM or 1 mM pyruvate, with images of representative wells. **E)** Relative viability of MiaPaCa-2 knockdown cells after treatment with 5 μM UK5099 and culture in DMEM, 1 mM pyruvate, or CAF CM. **F)** Relative colony formation of MiaPaCa-2 GOT2 knockdown cells cultured in DMEM, 1 mM pyruvate, or 1 mM lactate. Bars represent mean ± SD, *p<0.05, **p<0.01, ***p<0.001, ****p<0.0001.

Pyruvate can be converted to Acetyl-CoA in the mitochondria by pyruvate dehydrogenase (PDH), where it enters the TCA cycle. Therefore, GOT2 knockdown cells were cultured with CAF CM or pyruvate in the presence of the mitochondrial pyruvate carrier (MPC) inhibitor UK5099, which blocks entry of pyruvate into the mitochondria. Both CAF CM and pyruvate retained the ability to rescue colony formation in cells with GOT2 knockdown in the presence of UK5099 (**Fig.4E**). Next, we examined lactate since it is found at millimolar concentrations in tumors and can be converted to pyruvate, as well as having the potential to be used as a carbon source for the TCA cycle[33]. Unlike pyruvate, lactate did not rescue colony formation following GOT2 knockdown (**Fig.4F**). Additionally, our group discovered previously that CAFs release alanine, which is taken up by cancer cells and converted to pyruvate in the mitochondria by mitochondrial alanine aminotransaminase to fuel the TCA cycle[18]. Alanine similarly failed to rescue GOT2 knockdown (**Extended Data Fig.4H**). These data collectively indicated that even though GOT2 knockdown disrupts mitochondrial metabolism, pyruvate does not need to enter

bioRxiv preprint doi: https://doi.org/10.1101/2020.08.07.238766; this version posted August 7, 2020. The copyright holder for this preprint (which was not certified by peer review) is the author/funder, who has granted bioRxiv a license to display the preprint in perpetuity. It is made available under aCC-BY-NC-ND 4.0 International license.

the mitochondria, and it appears that pyruvate is not directly participating in mitochondrial anaplerosis to promote colony formation.

GOT2 knockdown perturbs redox homeostasis in PDA cells

GOT2 is part of the MAS (**Fig.1A**), a central metabolic mechanism by which cells transfer reducing equivalents between the cytosol and mitochondria. In cultured PDA cells, the MAS transfers glycolytic reducing potential to drive the electron transport chain (ETC) and maintain redox balance. We thus hypothesized that GOT2 knockdown interrupted this shuttle, preventing the proper transfer of electron potential in the form of NADH between these two compartments. Indeed, GOT2 knockdown increased the intracellular ratio of NADH to NAD+ (**Fig.5A**). Also, re-examination of the metabolomics dataset from cells with GOT2 knockdown revealed an impairment in glycolysis with a node at glyceraldehyde 3-phosphate dehydrogenase (GAPDH) (**Fig.5B**). GAPDH reduces NAD+ to produce NADH, where a build-up of NADH would serve to product-inhibit GAPDH activity. Indeed, this explains the metabolic signature observed, where upstream glycolysis, and branch pathways like the pentose phosphate pathway, are increased, while downstream glycolysis is decreased (**Fig.5C**). On the contrary, this effect on glycolysis was not observed in the metabolomics analysis from subcutaneous GOT2 knockdown tumors, further illustrating the differential dependence on GOT2 in PDA in vitro and in vivo (**Extended Data Fig.5A**). The Seahorse glycolytic rate assay confirmed that glycolysis was indeed impaired during GOT2 knockdown in vitro (**Extended Data Fig.5B**).

Pyruvate restores redox balance after GOT2 knockdown

NADH stress can be relieved if the cell has access to electron acceptors[25]. Pyruvate can accept electrons from NADH, producing lactate and regenerating NAD+ in a reaction catalyzed by lactate dehydrogenase (LDH). Since GOT2 knockdown caused a build-up of NADH, we hypothesized that this is the mechanism by which pyruvate rescues colony formation. To test this, GOT2 knockdown cells were cultured with α-ketobutyrate (αKB), another electron acceptor that turns over NADH in a mechanism analogous to pyruvate without acting in downstream metabolism in the same fashion as pyruvate[27]. In support of our hypothesis, αKB also rescued colony formation after GOT2 knockdown (**Fig.5D; Extended Data Fig.5C**).

To test this further, GOT2 knockdown cells were generated to express either doxycycline-inducible cytosolic or mitochondrial Lactobacillus brevis NADH oxidase (LbNOX), which uses molecular oxygen to oxidize NADH and produce water and NAD+ (**Extended Data Fig.5D**)[34,35]. Cytosolic LbNOX, but not mitochondrial LbNOX, rescued colony formation imparted by GOT2 knockdown (**Fig.5E; Extended Data Fig.5E**). Curiously, the spatial control of this LbNOX system indicated that knock down of mitochondrial GOT2 could be rescued by balancing the cytosolic NADH/NAD+ pool. Lastly, rescue of GOT2 knockdown requires the relief of NADH stress, as opposed to increased production of NAD+, as supplementation with the NAD+ precursor nicotinamide mononucleotide (NMN) did not rescue GOT2 knockdown (**Extended Data Fig.5F**).

These findings provide clear evidence that GOT2 knockdown results in a build-up of NADH pools and redox stress in PDA cells. Similarly, it has been well-established that inhibiting the activity of complex I of the ETC also results in an increase in NADH, which can be counteracted

bioRxiv preprint doi: https://doi.org/10.1101/2020.08.07.238766; this version posted August 7, 2020. The copyright holder for this preprint (which was not certified by peer review) is the author/funder, who has granted bioRxiv a license to display the preprint in perpetuity. It is made available under aCC-BY-NC-ND 4.0 International license.

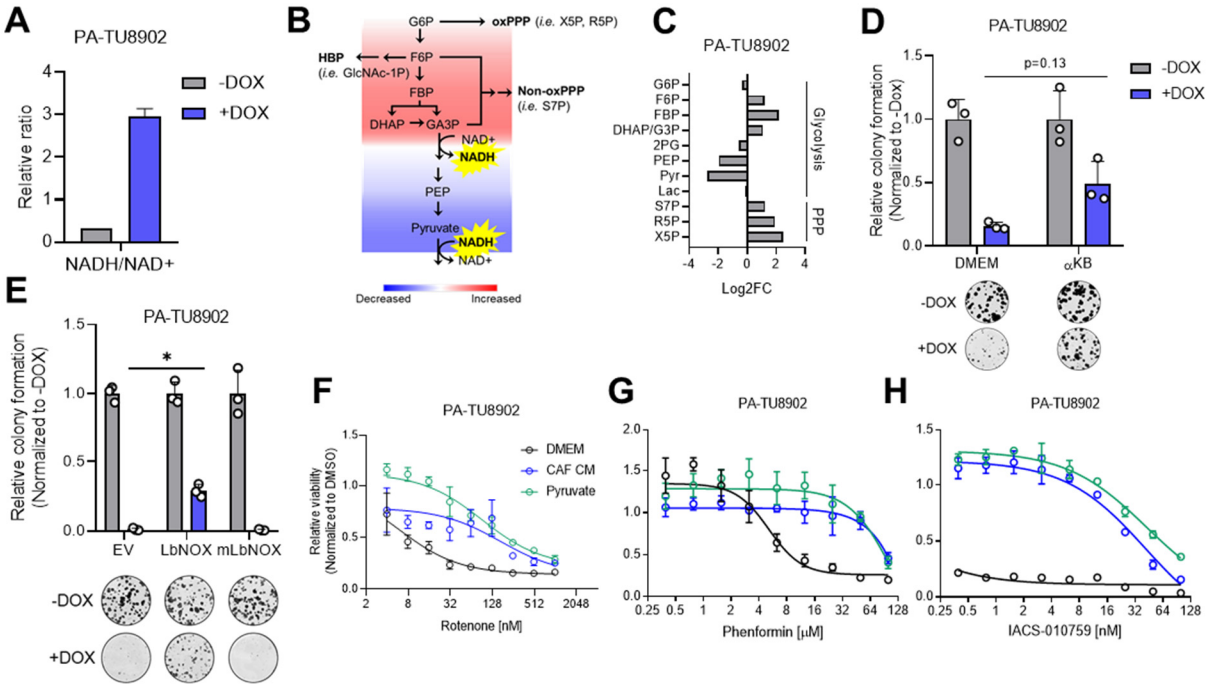

Fig.5 GOT2 knockdown disturbs redox homeostasis, which is restored by extracellular pyruvate. **A)** Relative ratio of NADH/NAD+ in PA-TU8902 GOT2 knockdown cells. **B)** Schematic summarizing the metabolomics data upon GOT2 knockdown depicting the effects of an increase in NADH levels on glycolysis. **C)** Log2 fold change of glycolytic and pentose phosphate pathway intermediates in PA-TU8902 GOT2 knockdown cells. **D)** Relative colony formation of PA-TU8902 GOT2 knockdown cells cultured in DMEM or 1 mM αKB, with images of representative wells. **E)** Relative colony formation of PA-TU8902 GOT2 knockdown cells expressing cytosolic or mitochondrial LbNOX. **F-H)** Relative viability of PA-TU8902 cells cultured in DMEM, 75% CAF CM, or 1 mM pyruvate and treated with rotenone (F), phenformin (G), or IACS-010759 (H). Bars represent mean ± SD, *p<0.05, **p<0.01, ***p<0.001, ****p<0.0001. Glucose-6-phosphate (G6P), fructose-6-phosphate (F6P), fructose-1,6-bisphosphate (FBP), dihydroxyacetone phosphate (DHAP), glyceraldehyde-3-phosphate (G3P), 2-phosphoglycerate (2PG), phosphoenol pyruvate (PEP), pyruvate (Pyr), lactate (Lac), sedoheptulose-7-phosphate (S7P), ribose-5-phosphate (R5P), xylulose-5-phosphate (X5P).

with extracellular pyruvate[25,27,30,35]. Therefore, since pyruvate is highly abundant in CAF CM, we hypothesized that PDA cells cultured in CAF CM would be protected from complex I inhibitors. Indeed, both CAF CM and extracellular pyruvate conferred resistance to PDA cells against the complex I inhibitors rotenone, phenformin, and IACS-010759 (**Fig.5F-H**)[36].

Blocking monocarboxylate transporter 1 (MCT1) prevents pyruvate and CAF CM rescue of GOT2 knockdown

According to our model, PDA cells could be more vulnerable to GOT2 knockdown or complex I inhibitors in a pyruvate-depleted environment, or if pyruvate uptake were blocked. Pyruvate is transported by four MCT isoforms[37-39], and an analysis of the CCLE database suggests that PDA cell lines primarily express MCT1 and MCT4 (**Extended Data Fig.6A**). Since MCT1 has a higher affinity for pyruvate than MCT4[38], we decided to focus on MCT1 as the transporter by which PDA cells import pyruvate. Indeed, PDA cells express significantly higher levels of MCT1

bioRxiv preprint doi: https://doi.org/10.1101/2020.08.07.238766; this version posted August 7, 2020. The copyright holder for this preprint (which was not certified by peer review) is the author/funder, who has granted bioRxiv a license to display the preprint in perpetuity. It is made available under aCC-BY-NC-ND 4.0 International license.

as compared to CAFs (**Extended Data Fig.6B**). Similarly, examining expression of MCT1 from a recently published single cell analysis of a murine syngeneic orthotopic pancreatic tumor (Steele, et al. *Nature Cancer*, accepted July 2020) indicated that PDA cells express high levels of MCT1 (**Extended Data Fig.6C**).

Based on these expression data, we hypothesized that blocking pyruvate import through MCT1 would render cells vulnerable to GOT2 knockdown or complex I inhibition. The small molecule AZD3965 has specificity for MCT1 over MCT4[40,41], therefore GOT2 knockdown cells were cultured in pyruvate or CAF CM in the presence of AZD3965. In support of our hypothesis, neither pyruvate nor CAF CM rescued GOT2 knockdown with MCT1 chemical inhibition (**Fig.6A,B**). Similarly, disrupting MCT1 with CRISPR-Cas9 in GOT2 knockdown cells prevented pyruvate rescue (**Fig.6C,D**). Interestingly, MCT1 inhibition was most effective at physiological levels of pyruvate (250 μM)(**Fig.6B,D**). In parallel to experiments with GOT2 knockdown, MCT1 blockade was tested in combination with complex I inhibitors in PDA cells cultured in pyruvate or CAF CM. AZD3965 also reversed the rescue activity of pyruvate or CAF CM in PDA cells treated with IACS-010759 (**Fig.6E**). Cumulatively, these data support a model where perturbation of mitochondrial metabolism with GOT2 knockdown or complex I inhibition disrupts redox balance in PDA cells, which can be restored through import of pyruvate from the tumor microenvironment and reduction to lactate to oxidize NADH and regenerate NAD+ (**Fig.6F**).

DISCUSSION

GOT2 is an essential component of the MAS and required for redox homeostasis in PDA. Knockdown of GOT2 disrupts this shuttle and renders PDA cells incapable of transferring reducing equivalents between the cytosol and mitochondria, leading to a cytosolic build-up of NADH. This predominantly impacts the rate of glycolysis, an NAD+-coupled pathway, with secondary impacts on mitochondrial metabolism, that together slow the proliferation of PDA cells in vitro. Extracellular supplementation with electron acceptors like pyruvate and αKB, or the expression of a cytosolic NADH oxidase, relieves NADH stress and pathway feedback inhibition. According to the data presented herein, GOT2 knockdown does not affect the growth of PDA tumors in vivo because electron acceptors in the tumor microenvironment can restore redox homeostasis. Indeed, pyruvate is present in mouse serum at 250 μM[23], a concentration which is sufficient to compensate for GOT2 knockdown in vitro. Furthermore, we have shown that pancreatic CAFs release pyruvate, which is taken up and utilized by PDA cells. This is supported by previous findings in CAFs from other cancers[42]. Therefore, a source of pyruvate, either from CAFs or from the circulation, is available to PDA tumors. Finally, blocking pyruvate uptake deprives PDA cells of a critical means to relieve the NADH stress mediated by GOT2 knockdown dampening the pyruvate or CAF CM rescue activity.

Aside from its broader role in redox balance, GOT2 is also a prominent source of aspartate in PDA cells, since knock down of GOT2 dramatically decreases aspartate levels both in vitro and in vivo. Previous studies have shown that aspartate availability is rate limiting in rapidly proliferating cells[26-28,30]. Surprisingly, even supraphysiological levels of aspartate as a single agent did not rescue GOT2 knockdown, and simultaneous treatment with supraphysiological doses of both Asp and αKG were required to provide a partial rescue of PDA cell proliferation in the absence of GOT2. Accordingly, this suggests that Asp does not participate in the ability to

bioRxiv preprint doi: https://doi.org/10.1101/2020.08.07.238766; this version posted August 7, 2020. The copyright holder for this preprint (which was not certified by peer review) is the author/funder, who has granted bioRxiv a license to display the preprint in perpetuity. It is made available under aCC-BY-NC-ND 4.0 International license.

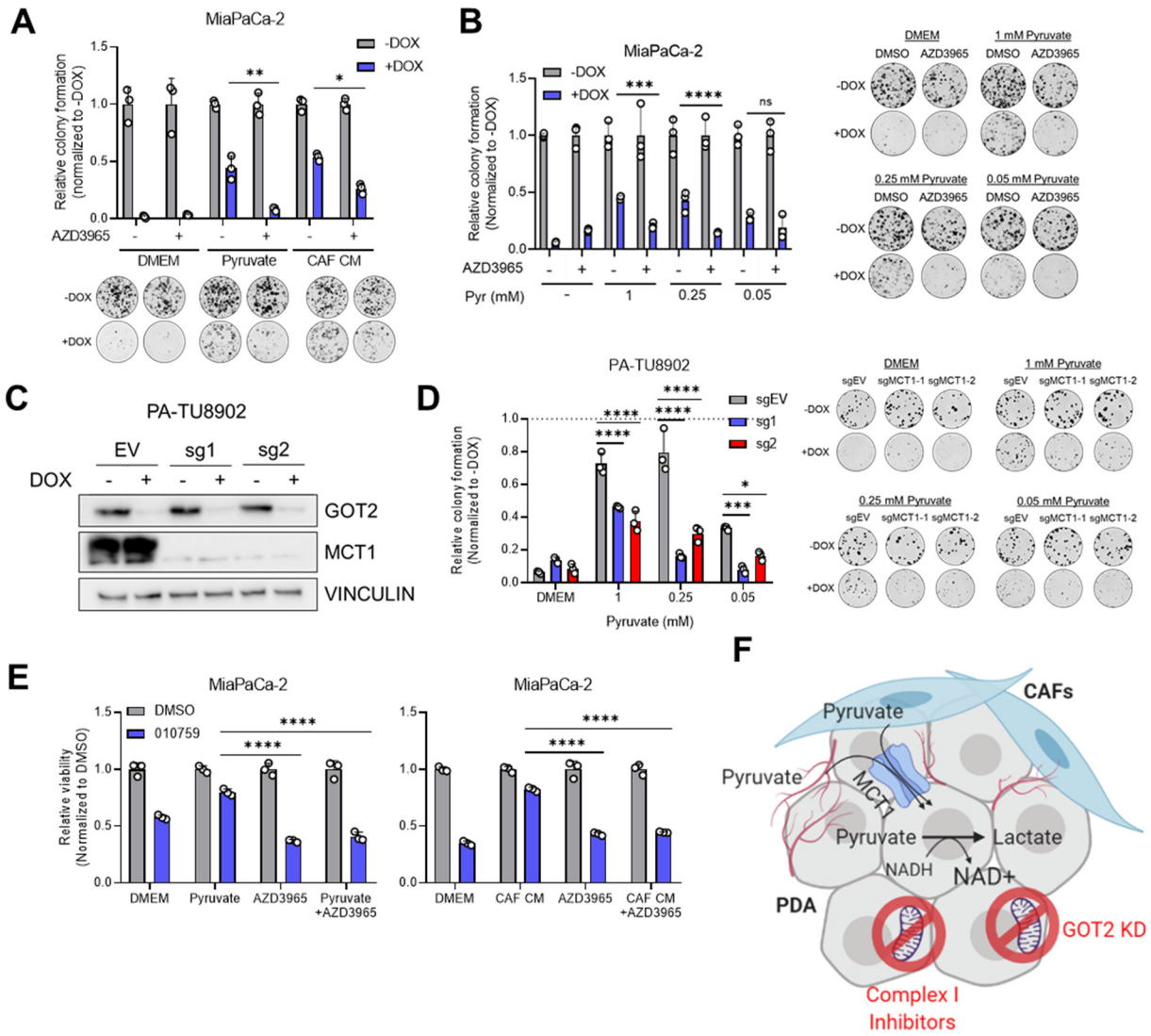

Fig.6 Blocking pyruvate uptake in vitro sensitizes PDA cells to redox disruption. A) Relative colony formation of MiaPaCa-2 shGOT2-1 cells treated with 100 nM AZD3965 and cultured in DMEM, 0.25 mM pyruvate, or CAF CM, with images of representative wells. **B)** Relative colony formation of MiaPaCa-2 GOT2 knockdown cells treated with 100 nM AZD3965 and cultured in DMEM or the indicated doses of pyruvate, with images of representative wells. **C)** Western blot for GOT2 and MCT1, with Vinculin loading control, in PA-TU8902 GOT2 knockdown, MCT1 knockout cells. **D)** Relative colony formation of PA-TU8902 shGOT2-1 MCT1 knockout cells cultured in DMEM or with the indicated doses of pyruvate, with images or representative wells. **E)** Relative viability of MiaPaCa-2 cells treated with 100 nM IACS-010759 and 100 nM AZD3965 and cultured in DMEM, 1 mM pyruvate, or CAF CM. **F)** Working model depicting the redox imbalance induced by GOT2 knockdown or complex I inhibition, which is then corrected through uptake of pyruvate released from CAFs or circulating through the vasculature. Bars represent mean ± SD, *p<0.05, **p<0.01, ***p<0.001, ****p<0.0001.

sustain tumor growth upon GOT2 knockdown in vivo, based on its availability at low micromolar concentrations and the limited uptake capacity of PDA cells[23]. Finally, supplementation of nucleosides similarly failed to rescue GOT2 knockdown. Therefore, we propose that the mechanism by which GOT2 knockdown slows PDA proliferation is through disruption of redox balance and deprivation of Asp. Supplying PDA cells with Asp meets a vital requirement for

bioRxiv preprint doi: https://doi.org/10.1101/2020.08.07.238766; this version posted August 7, 2020. The copyright holder for this preprint (which was not certified by peer review) is the author/funder, who has granted bioRxiv a license to display the preprint in perpetuity. It is made available under aCC-BY-NC-ND 4.0 International license.

pyrimidine biosynthesis but does not address the redox imbalance. Pyruvate, on the other hand, regenerates NAD+ allowing broader metabolic processes to resume, including Asp production. In support of this, recent work in myoblasts demonstrated that while complex I inhibition with piericidin increased the NADH/NAD+ ratio leading to depletion of Asp, adding Asp back to the system neither restored redox balance nor induced proliferation[43].

Our work also highlights the metabolic role of cancer-associated fibroblasts (CAFs) in PDA. Recent studies have shown that CAFs engage in cooperative metabolic crosstalk with cancer cells in many different tumor types[16,18,19,44,45]. We add to this body of literature by demonstrating that CAFs release pyruvate, which is taken up and utilized by PDA cells. However, much remains to be discovered about CAF metabolism. Some types of activated fibroblasts are known to be highly glycolytic[21,22], an observation supported by our data. Yet the advent of single-cell RNA sequencing in murine pancreatic tumor models has led to a recent appreciation for the heterogeneity of CAFs[46-49]. The newly identified iCAF, myCAF, and apCAF populations have distinct functions in a pancreatic tumor[46] and likely employ distinct metabolism to carry out these functions. Our future work will endeavor to uncover competitive or cooperative interactions between PDA cells and the various CAF subpopulations, including which subtype(s) are responsible for pyruvate release.

Perhaps most importantly, this work emphasizes that the role of the tumor microenvironment must be considered when targeting cancer metabolism. Extracellular pyruvate serves to buffer redox imbalances induced by targeting mitochondrial metabolism. Indeed, approaches like disrupting the MAS shuttle via GOT2 knockdown or blocking complex I with small molecule inhibitors were less effective when PDA cells were cultured in supplemental pyruvate or in CAF CM. These data are relevant since numerous mitochondrial inhibitors are currently in clinical trials against solid tumor types (NCT03291938, NCT03026517, NCT03699319, NCT02071862). Previous studies have also shown that complex I inhibitors are more effective in combination with AZD3965[50], a selective inhibitor of MCT1. Furthermore, the abundance of CAFs present in a tumor, as well as the level of circulating pyruvate in the patient, could predict outcomes for treatment with metabolic therapies that lead to redox imbalance. Targeting pancreatic cancer metabolism is an alluring approach, and a more detailed understanding of the metabolic crosstalk occurring in a pancreatic tumor can shed light on potential resistance mechanisms and inform more effective metabolic therapies.

Acknowledgements: This work was funded by T32AI007413 and F31CA24745701 (SAK); CA148828 and CA245546 (YMS); a Pancreatic Cancer Action Network/AACR Pathway to Leadership award (13-70-25-LYSS), Junior Scholar Award from The V Foundation for Cancer Research (V2016-009), Kimmel Scholar Award from the Sidney Kimmel Foundation for Cancer Research (SKF-16-005), a 2017 AACR NextGen Grant for Transformative Cancer Research (17-20-01-LYSS), and NIH grants R37CA237421, R01CA248160, R01CA244931 (CAL).

Additional funding sources include T32-DK094775 and T32-CA009676 (BSN); T32-GM11390 and F31-CA247076 (SBK); T32-CA009676, the American Cancer Society Postdoctoral Award PF-19-096-01, and the Michigan Institute for Clinical and Healthy Research (MICHR) Postdoctoral Translational Scholar Program fellowship award (NGS); the Michigan Postdoctoral Pioneer Program (ZCN); K99CA241357 and P30DK034933 (CJH); R01GM101171 (DBL); and Cancer Center support grant (P30 CA046592).

bioRxiv preprint doi: https://doi.org/10.1101/2020.08.07.238766; this version posted August 7, 2020. The copyright holder for this preprint (which was not certified by peer review) is the author/funder, who has granted bioRxiv a license to display the preprint in perpetuity. It is made available under aCC-BY-NC-ND 4.0 International license.

Metabolomics studies performed at the University of Michigan were supported by NIH grant DK097153, the Charles Woodson Research Fund, and the UM Pediatric Brain Tumor Initiative.

Author contributions: SAK, YMS, and CAL conceived of and designed this study. SAK, YMS, and CAL planned and guided the research and wrote the manuscript. SAK, LL, ALM, BC, PS, AR, GT, BSN, SBK, NGS, MTH, HW, DL, SEA, JR, XG, LZ, AA, ZCN, SG, CJH, DBL, HCC, MPdM, YMS, and CAL provided key reagents, performed experiments, analyzed, and interpreted data. YMS and CAL supervised the work carried out in this study.

Declaration of Interests: CAL is an inventor on patents pertaining to Kras regulated metabolic pathways, redox control pathways in pancreatic cancer, and targeting the GOT1-pathway as a therapeutic approach.

MATERIALS AND METHODS

Cell culture: MiaPaCa-2, BxPC-3, Capan-1, Panc03.27, Panc10.05, PL45, and HPNE cell lines were obtained from ATCC. PA-TU8902, PA-TU8988T, and YAPC cells lines were obtained from DSMZ. UM6, UM19, UM28, UM32, UM53, and UM76 were generated from primary patient tumors at the University of Michigan. Human pancreatic stellate cells (hPSCs, also described here as CAFs) were a generous gift from Rosa Hwang[51]. All cell lines were cultured in high-glucose Dubelcco's Modified Eagle Medium (DMEM, Gibco) without pyruvate and supplemented with 10% fetal bovine serum (FBS, Corning). 0.25% Trypsin (Gibco) was used to detach and passage cells. Cell lines were tested regularly for mycoplasma contamination using MycoAlert (Lonza). All cell lines in this study were validated for authentication using STR profiling via the University of Michigan Advanced Genomics Core. L-Aspartic acid (Sigma), dimethyl-α-ketoglutarate (Sigma), sodium pyruvate (Invitrogen), α-ketobutyrate (Sigma), nicotinamide mononucleotide (NMN, Sigma), L-alanine (Sigma), and sodium lactate (Sigma) were used at the indicated concentrations. UK5099, AZD3965, and phenformin were purchased from Cayman chemical, rotenone from Sigma, and IACS-010759 was a generous gift from Dr. Haoqiang Ying.

Doxy-inducible shGOT2 cells: The following shRNA sequences against GOT2 were purchased from Sigma and cloned into the Tet-pLKO-puro lentiviral vector (Addgene, #21915): sh1-TRCN0000034824 and sh2-TRCN0000034825. A non-targeting sequence was used as a control (shNT). Tet-pLKO-shGOT2 and tet-pLKO-shNT lentiviruses were produced by the University of Michigan Vector Core using purified plasmid DNA. Stable cell lines were generated through transduction with optimized viral titers and selection with 2 μg/mL puromycin for 7 days.

GOT2 knockout cells: GOT2 knockout PDA cell lines were generated using a CRISPR-Cas9 method described previously[52]. Briefly, sgRNA oligonucleotide pairs obtained from the Human Gecko Library (v2, 3/9/2015) (sg1 (Fwd) 5'-CACCgAAGCTCACCTTGCGGACGCT-3', (Rev) 5'-AAACAGCGTCCGCAAGGTGAGCTTc; sg2 (Fwd) 5'-CACCgCGTTCTGCCTAGCGTCCGCA-3', (Rev) 5'-AAACTGCGGACGCTAGGCAGAACGc-3') were cloned into the pSpCas9(BB)-2A-Puro plasmid (PX459, v2.0; Addgene, #62988), transfected in PDA cell lines, and selected in puromycin for 7 days. Cells were then seeded into 24 well plates at a density of 1 cell per well, and individual clones were expanded. GOT2 knockout was verified via Western blot. Cells transfected with the empty PX459 vector were used as controls.

Transduction of LbNOX/mitoLbNOX: pINDUCER (Addgene, #44014) plasmids containing GFP, LbNOX, or mitoLbNOX were a generous gift from Dr. Haoqing Yang (MD Anderson). Plasmids

bioRxiv preprint doi: https://doi.org/10.1101/2020.08.07.238766; this version posted August 7, 2020. The copyright holder for this preprint (which was not certified by peer review) is the author/funder, who has granted bioRxiv a license to display the preprint in perpetuity. It is made available under aCC-BY-NC-ND 4.0 International license.

were sequenced and transfected along with lentiviral packaging plasmids into HEK293FT cells with Lipofectamine 3000 (Thermo Fisher) per manufacturer's instructions. Virus was collected after 48 hours and filtered through a 0.2 µm filter. PA-TU8902 and MiaPaCa-2 shGOT2-1 cells were seeded in 6 well plates at 250,000 cells/well, transduced with the indicated vectors, and selected in G418 at 500 µg/mL for 7 days. Expression of Flag-tagged LbNOX or mitoLbNOX was confirmed by Western blot with a Flag antibody after culturing cells in 1 µg/mL doxycycline for 3 days.

Luciferase-expressing cells: MiaPaCa-2 GOT2 knockdown cells were transduced with the FUGW-FL (EF1a-luc-UBC6-EGFP) lentiviral vector constructed previously[53] and GFP+ cells were selected via flow cytometry. Luciferase activity was confirmed following transduction and selection with an in vitro luciferase assay and detection on a SpectraMax M3 Microplate reader (Molecular Devices).

ATP fluorescent sensor: GOT2 knockdown cells were transduced with CytoATP or CytoATP non-binding control vectors using the CytoATP Lentivirus Reagent Kit (Sartorious, #4772) and polybrene transfection reagent (Thermo Fisher) and selected for 7 days in 2 µg/mL puromycin. For proliferation and rescue experiments, cells were incubated in an Incucyte (Sartorious) equipped with a Metabolism Optical Module, where the ratio of ATP binding was detected and normalized to the non-binding control cells. Proliferation rate was determined by the percent confluence detected in the phase channel of the Incucyte normalized to Day 0 for each condition.

Conditioned media: Conditioned media was generated by splitting cells at ~90% confluence in a 10 cm^2 plate into four 15 cm^2 plates containing a final volume of 27 mL of growth media, and incubating for 72 hours at 37°C, 5% CO_2. After, the media was collected in 50 mL conical tubes, centrifuged at 1,000 rpm for 5 minutes to remove any detached cells or debris, and divided into fresh 15 mL conical tubes in 10 mL aliquots before long-term storage at -80°C. For all conditioned media experiments, unless indicated otherwise, growth media was mixed with conditioned media for a final ratio of 75% conditioned media to 25% fresh growth media.

For the experiments in Fig.3 and Extended Data Fig.3, conditioned media were manipulated as follows. For boiling, the conditioned media tubes were placed in a water bath at 100°C for 10 minutes. To filter out factors >3 kDa, the conditioned media were transferred to a 3 kDa filter (Millipore) and centrifuged at 15,000 rpm in 30-minute increments until all the conditioned media had passed through the filter. To expose the conditioned media to freeze-thaw cycles, the tubes containing the conditioned media were thawed for 30 minutes in a 60°C water bath, and then frozen at -80°C for 30 minutes. This was repeated two more times for a total of three freeze-thaw cycles.

Colony formation assays: Cells were seeded in 6 well plates at 200-400 cells per well in 2 mL of growth media and incubated overnight at 37°C, 5% CO_2. The next day, the growth media was aspirated and fresh media containing the indicated compounds were added to the cells. Doxycycline was used at 1 µg/mL for all assays. For each assay, cells were incubated in the indicated conditions for 10 days, with the media and doxycycline changed every three days. After 10 days, the media was aspirated, the wells were washed once with PBS, and the cells were fixed in 100% methanol for 10 minutes. Next, the methanol was removed, and the cells were stained with 0.4% crystal violet for 10 minutes. Finally, the crystal violet was removed, the plates were washed under running water and dried on the benchtop overnight. The next day,

bioRxiv preprint doi: https://doi.org/10.1101/2020.08.07.238766; this version posted August 7, 2020. The copyright holder for this preprint (which was not certified by peer review) is the author/funder, who has granted bioRxiv a license to display the preprint in perpetuity. It is made available under aCC-BY-NC-ND 4.0 International license.

images were taken of the plates with a Chemidoc BioRad imager and quantified using the ColonyArea plugin in ImageJ as described previously[54].

CyQUANT viability assay: Cells were seeded in 96 well black wall, clear bottom plates at 2,000 cells/well in 50 µL of media and incubated overnight at 37°C, 5% CO_2. The next day, 150 µL of the indicated treatment media was added to the appropriate wells, and the cells were incubated for 4 more days. At endpoint, the media was removed from the wells, and the plates were stored overnight at -80°C. The next day, proliferation was determined by CyQUANT (Invitrogen) according to the manufacturer's instructions, and fluorescence was detected on a SpectraMax M3 Microplate reader (Molecular Devices).

Glycolytic rate assay: PA-TU8902 GOT2 knockdown cells that had been cultured in 1 µg/mL doxycycline for 3 days were seeded at $2x10^4$ cells/well in 80 µl/well of normal growth media in an Agilent XF96 V3 PS Cell Culture Microplate (Agilent). To achieve an even distribution of cells within wells, plates were incubated on the bench top at room temperature for 1 hour before incubating at 37ºC, 5% CO_2 overnight. To hydrate the XF96 FluxPak (Agilent), 200 µL/well of sterile water was added and the entire cartridge was incubated at 37ºC, CO_2-free incubator overnight. The following day, one hour prior to running the assay, 60 µL of media was removed, and the cells were washed twice with 200 µL/well of assay medium (XF DMEM Base Medium, pH 7.4 containing 25 mM Glucose and 4 mM Glutamine; Agilent). After washing, 160 µL/well of assay medium was added to the cell culture plate for a final volume of 180 µL/well. Cells were then incubated at 37ºC, in a CO_2-free incubator until analysis. In parallel, one hour prior to the assay, water from the FluxPak hydration was exchanged for 200 µL/well of XF Calibrant 670 (Agilent) and the cartridge was returned to 37ºC, CO_2-free incubator until analysis. Rotenone/Antimycin (50 µM, Agilent) and 2DG (500 mM, Agilent) were re-constituted in assay medium to make the indicated stock concentrations. 20 µL of rotenone/antimycin was loaded into Port A for each well of the FluxPak and 22 µL of 2DG into Port B, for a final concentration of 0.5 µM and 50 mM, respectively. The Glycolytic Rate Assay was conducted on an XF96 Extracellular Flux Analyzer (Agilent) and PER was calculated using Wave 2.6 software (Agilent). Following the assay, PER was normalized to cell number with the CyQUANT NF Cell Proliferation Assay (Invitrogen) according to manufacturer's instructions.

Protein lysates: Cell lines cultured in 6 well plates in vitro were washed with ice-cold PBS on ice and incubated in 250 µL of RIPA buffer (Sigma) containing protease (Roche) and phosphatase (Sigma) inhibitors on ice for 10 minutes. Next, cells were scraped with a pipet tip, and the resulting lysate was transferred to a 1.5 mL tube also on ice. The lysate was centrifuged at 15,000 rpm for 10 minutes at 4°C. After, the supernatant was transferred to a fresh 1.5 mL tube and stored at -80°C.

In vivo tumor tissue was placed in a 1.5 mL tube containing a metal ball and 300 µL RIPA buffer with protease and phosphatase inhibitors. The tissue was homogenized using a tissue lyser machine. Then, the resulting lysate was centrifuged at 15,000 rpm for 10 minutes at 4°C. After, the supernatant was transferred to a fresh 1.5 mL tube and stored at -80°C.

Western blotting: Protein levels were determined using a BCA assay (Thermo Fisher), according to manufacturer's instructions. Following quantification, the necessary volume of lysate containing 30 µg of protein was loading dye (Invitrogen) and reducing agent (Invitrogen) and incubated at 90°C for 5 minutes. Next, the lysate separated on a 4-12% Bis-Tris gradient gel (Invitrogen) along with a protein ladder (Invitrogen) at 150 V until the dye reached the

bioRxiv preprint doi: https://doi.org/10.1101/2020.08.07.238766; this version posted August 7, 2020. The copyright holder for this preprint (which was not certified by peer review) is the author/funder, who has granted bioRxiv a license to display the preprint in perpetuity. It is made available under aCC-BY-NC-ND 4.0 International license.

bottom of the gel (about 90 minutes). Then, the protein was transferred to a methanol-activated PVDF membrane (Millipore) at 25 V for 1 hour. After that, the membrane was blocked in 5% blocking reagent (Biorad) dissolved in TBS-T rocking for > 1 hour. Next, the membrane was incubated overnight at 4°C rocking in the indicated primary antibody diluted in blocking buffer. The next day, the primary antibody was removed, and the membrane was washed 3 times in TBS-T rocking for 5 minutes. Then, the membrane was incubated for 1 hour rocking at room temperature in the appropriate secondary antibody diluted in TBS-T. Finally, the membrane was washed as before, and incubated in Clarity ECL reagent (Biorad) according to manufacturer's instructions before imaging on a Biorad Chemidoc. The following primary antibodies were used in this study: GOT2 (Atlas, HPA018139), GOT1 (Abcam, ab171939), GLUD1 (Abcam, ab166618), IDH1 (Cell Signaling, 3997S), MCT1 (Abcam, ab85021), anti-Flag (Sigma, F3165), Vinculin (Cell Signaling, 13901S), and the anti-rabbit-HRP secondary antibody (Cell Signaling, 7074S)

Isolating polar metabolites: For intracellular metabolome analyses, cells were seeded at 10,000 cells in 2 mL of growth media per well of a 6 well plate and incubated overnight. The next day, the growth media was removed, and cells were incubated in media containing the indicated compounds for 6 days, with the media being changed every 3 days. On day 6, the media was removed, and the cells were incubated in 1 mL/well of ice-cold 80% methanol on dry ice for 10 minutes. Following the incubation, the wells were scraped with a pipet tip and transferred to a 1.5 mL tube on dry ice.

To analyze extracellular metabolomes, 0.8 mL of ice-cold 100% methanol was added to 0.2 mL of media, mixed well, and incubated on dry ice for 10 minutes.

The tubes were then centrifuged at 15,000 rpm for 10 minutes at 4°C, and the resulting metabolite supernatant was transferred to a fresh 1.5 mL tube. The metabolites were then dried on a SpeedVac until all the methanol had evaporated, and re-suspended in a 50:50 mixture of methanol and water.

Snapshot metabolomics: Samples were run on an Agilent 1290 Infinity II LC -6470 Triple Quadrupole (QqQ) tandem mass spectrometer (MS/MS) system with the following parameters: Agilent Technologies Triple Quad 6470 LC-MS/MS system consists of the 1290 Infinity II LC Flexible Pump (Quaternary Pump), the 1290 Infinity II Multisampler, the 1290 Infinity II Multicolumn Thermostat with 6 port valve and the 6470 triple quad mass spectrometer. Agilent Masshunter Workstation Software LC/MS Data Acquisition for 6400 Series Triple Quadrupole MS with Version B.08.02 is used for compound optimization, calibration, and data acquisition.

Solvent A is 97% water and 3% methanol 15 mM acetic acid and 10 mM tributylamine at pH of 5. Solvent C is 15 mM acetic acid and 10 mM tributylamine in methanol. Washing Solvent D is acetonitrile. LC system seal washing solvent 90% water and 10% isopropanol, needle wash solvent 75% methanol, 25% water. GC-grade Tributylamine 99% (ACROS ORGANICS), LC/MS grade acetic acid Optima (Fisher Chemical), InfinityLab Deactivator additive, ESI –L Low concentration Tuning mix (Agilent Technologies), LC-MS grade solvents of water, and acetonitrile, methanol (Millipore), isopropanol (Fisher Chemical).

An Agilent ZORBAX RRHD Extend-C18, 2.1 × 150 mm and a 1.8 um and ZORBAX Extend Fast Guards for UHPLC are used in the separation. LC gradient profile is: at 0.25 ml/min, 0-2.5 min, 100% A; 7.5 min, 80% A and 20% C; 13 min 55% A and 45% C; 20 min, 1% A and 99% C; 24 min, 1% A and 99% C; 24.05 min, 1% A and 99% D; 27 min, 1% A and 99% D; at 0.8 ml/min,

bioRxiv preprint doi: https://doi.org/10.1101/2020.08.07.238766; this version posted August 7, 2020. The copyright holder for this preprint (which was not certified by peer review) is the author/funder, who has granted bioRxiv a license to display the preprint in perpetuity. It is made available under aCC-BY-NC-ND 4.0 International license.

27.5-31.35 min, 1% A and 99% D; at 0.6 ml/min, 31.50 min, 1% A and 99% D; at 0.4 ml/min, 32.25-39.9 min, 100% A; at 0.25 ml/min, 40 min, 100% A. Column temp is kept at 35 ℃, samples are at 4 ℃, injection volume is 2 µl.

6470 Triple Quad MS is calibrated with the Agilent ESI-L Low concentration Tuning mix. Source parameters: Gas temp 150 ℃, Gas flow 10 l/min, Nebulizer 45 psi, Sheath gas temp 325 ℃, Sheath gas flow 12 l/min, Capillary -2000 V, Delta EMV -200 V. Dynamic MRM scan type is used with 0.07 min peak width, acquisition time is 24 min. dMRM transitions and other parameters for each compounds are list in a separate sheets. Delta retention time of plus and minus 1 min, fragmentor of 40 eV and cell accelerator of 5 eV are incorporated in the method.

The MassHunter Metabolomics Dynamic MRM Database and Method was used for target identification. Key parameters of AJS ESI were: Gas Temp: 150 ℃, Gas Flow 13 l/min, Nebulizer 45 psi, Sheath Gas Temp 325 ℃, Sheath Gas Flow 12 l/min, Capillary 2000 V, Nozzle 500 V. Detector Delta EMV(-) 200.

The QqQ data were pre-processed with Agilent MassHunter Workstation QqQ Quantitative Analysis Software (B0700). Each metabolite abundance level in each sample was divided by the median of all abundance levels across all samples for proper comparisons, statistical analyses, and visualizations among metabolites. The statistical significance test was done by a two-tailed t-test with a significance threshold level of 0.05.

Heatmaps were generated and data clustered using Morpheus Matrix Visualization and analysis tool (https://software.broadinstitute.org/morpheus).

Pathway analyses were conducted using MetaboAnalyst (https://www.metaboanalyst.ca).

<u>13C-Glucose isotope tracing:</u> CAFs seeded were seeded in 6 well plates at $2x10^5$ cells/well and incubated for 72 hours in growth media containing U13C-Glucose (Cambridge Isotope Laboratories). Polar metabolites were extracted from the media and cells according to the method described above. Isotope tracing parameters were as follows:

Agilent Technologies Q-TOF 6530 LC/MS system consists of a 1290 Infinity II LC Flexible Pump (Quaternary Pump), 1290 Infinity II Multisampler, 1290 Infinity II Multicolumn Thermostat with 6 port valve and a 6530 Q-TOF mass spectrometer with a dual Assisted Jet Stream (AJI) ESI source. Agilent MassHunter Workstation Software LC/MS Data Acquisition for 6200 series TOF/6500 series Q-TOF Version B.09.00 Build 9.0.9044.a SP1 is used for calibration and data acquisition.

An Agilent ZORBAX RRHD Extend-C18, 2.1 × 150 mm and a 1.8 um and ZORBAX Extend Fast Guards for UHPLC are used in the separation. LC gradient profile is: at 0.25 ml/min, 0-2.0 min, 100% A; 12.00 min, 1% A and 99% C ; 16.00 min 1% A and 99% C; 18.00 min, 1% A and 99% D; 19.30 min, 1% A and 99% C; 19.90 min, 1% A and 99% D (0.80 ml/min); 22.45 min, 1% A and 99% D (0.8 ml/min); 22.65 min, 1% A and 99% D (0.4 ml/min); 29.35 min, 1% A and 99% D (0.4 ml/min); 29.45 min, 100% A (0.25 ml/min), 40 min. Column temp is kept at 35 ℃, samples are at 4 ℃, injection volume is 5 µl.

Solvent A is 97% water and 3% methanol 15 mM acetic acid and 10 mM tributylamine at pH of 5. Solvent C is 15 mM acetic acid and 10 mM tributylamine in methanol. Washing Solvent D is acetonitrile. LC system seal washing solvent 90% water and 10% isopropanol, needle wash solvent 75% methanol, 25% water.

bioRxiv preprint doi: https://doi.org/10.1101/2020.08.07.238766; this version posted August 7, 2020. The copyright holder for this preprint (which was not certified by peer review) is the author/funder, who has granted bioRxiv a license to display the preprint in perpetuity. It is made available under aCC-BY-NC-ND 4.0 International license.

Agilent 6530 Q-TOF MS is calibrated with ESI-L Low Concentration Tuning mix. Source parameters: Gas temp 250 ℃, Gas flow 13 l/min, Nebulizer 35 psi, Sheath gas temp 325 ℃, Sheath gas flow 12 l/min, Vcap 3500 V, Nozzle Voltage (V) 1500, Fragmentor 140, Skimmer1 65, OctopoleRFPeak 750. The MS acquisition mode is set in MS1 with mass range between 50-1200 da with collision energy of zero. The scan rate (spectra/sec) is set at 1 Hz. The LC-MS acquisition time is 18 min and total run time is 30 min. Reference masses are enabled with reference masses in negative mode of 112.9856 and 1033.9881 da.

Xenograft studies: Animal experiments were conducted in accordance with the Office of Laboratory Animal Welfare and approved by the Institutional Animal Care and Use Committees of the University of Michigan. NOD scid gamma (NSG) mice (Jackson Laboratory) 6-10 weeks old of both sexes were maintained in the facilities of the Unit for Laboratory Animal Medicine (ULAM) under specific pathogen-free conditions.

Cells expressing doxycycline-inducible shNT or shGOT2 were injected subcutaneously into both the left and right flanks of male and female NSG mice, with 200,000 cells in a mixture of 50 µL media and 50 µL Matrigel (Corning) per injection. Tumors were established for 7 days before mice were fed either normal chow or chow containing doxycycline (BioServ). Tumors were measured with calipers two times per week, and mice were euthanized once the tumors reached a volume of 2 cm^3. Subcutaneous tumor volume (V) was calculated as V=1/2(length x $width^2$). At endpoint, the tumors were removed, and fragments were either snap frozen in liquid nitrogen and stored at -80°C or fixed in ZFix solution (Anatech) for histology.

Cells expressing luciferase in addition to doxycycline-inducible shGOT2 were injected into the pancreas tail of NSG mice, with 200,000 cells in a mixture of 50 µL media and 50 µL Matrigel (Corning) per injection. Tumors were established for 7 days before mice were fed either normal chow or chow containing doxycycline (BioServ). Tumor progression was monitored by weekly intraperitoneal injections of luciferin (Promega) and bioluminescence imaging (BLI) on an IVIS SpectrumCT (Perkin Elmer). BLI was analyzed with Living Image software (PerkinElmer) At endpoint, the tumors were removed, and fragments were either snap frozen in liquid nitrogen and stored at -80°C or fixed in ZFix (Anatech) solution for histology.

Histology: Tissues were processed using a Leica ASP300S tissue processor (Leica Microsystems). Paraffin-embedded tissues were sectioned at 4 µm and stained for specific target proteins using the Discovery Ultra XT autostainer (Ventana Medical Systems), with listed antibodies, and counterstained with Mayer's hematoxylin (Sigma). Hematoxylin and eosin (H&E) staining was performed using Mayer's hematoxylin solution and Eosin Y (Thermo Fisher). IHC slides were then scanned on a Pannoramic SCAN scanner (Perkin Elmer). Scanned images were quantified using algorithms provided from Halo software version 2.0 (Indica Labs). The following antibodies were used for IHC: Ki67 (Abcam, ab15580), αSMA (Abcam, ab5694).

Statistics: Statistics were performed using Graph Pad Prism 8. Groups of 2 were analyzed with two-tailed students t test, groups greater than 2 were compared using one-way ANOVA analysis with Tukey post hoc test or two-way ANOVA with Dunnett's correction for multiple independent variables. All error bars represent mean with standard deviation, all group numbers and explanation of significant values are presented within the figure legends. Experiments were repeated twice to verify results.

bioRxiv preprint doi: https://doi.org/10.1101/2020.08.07.238766; this version posted August 7, 2020. The copyright holder for this preprint (which was not certified by peer review) is the author/funder, who has granted bioRxiv a license to display the preprint in perpetuity. It is made available under aCC-BY-NC-ND 4.0 International license.

REFERENCES

1 Pavlova, N. N. & Thompson, C. B. The Emerging Hallmarks of Cancer Metabolism. *Cell metabolism* **23**, 27-47, doi:10.1016/j.cmet.2015.12.006 (2016).

2 Vander Heiden, M. G. & DeBerardinis, R. J. Understanding the Intersections between Metabolism and Cancer Biology. *Cell* **168**, 657-669, doi:10.1016/j.cell.2016.12.039 (2017).

3 Vander Heiden, M. G. Targeting cancer metabolism: a therapeutic window opens. *Nature reviews. Drug discovery* **10**, 671-684, doi:10.1038/nrd3504 (2011).

4 Ryan, D. P., Hong, T. S. & Bardeesy, N. Pancreatic Adenocarcinoma. *New England Journal of Medicine* **371**, 1039-1049, doi:10.1056/NEJMra1404198 (2014).

5 Halbrook, C. J. & Lyssiotis, C. A. Employing Metabolism to Improve the Diagnosis and Treatment of Pancreatic Cancer. *Cancer Cell* **31**, 5-19, doi:10.1016/j.ccell.2016.12.006 (2017).

6 Kamphorst, J. J. *et al.* Human pancreatic cancer tumors are nutrient poor and tumor cells actively scavenge extracellular protein. *Cancer Res* **75**, 544-553, doi:10.1158/0008-5472.CAN-14-2211 (2015).

7 Commisso, C. *et al.* Macropinocytosis of protein is an amino acid supply route in Ras-transformed cells. *Nature* **497**, 633-637, doi:10.1038/nature12138 (2013).

8 Ying, H. *et al.* Oncogenic Kras maintains pancreatic tumors through regulation of anabolic glucose metabolism. *Cell* **149**, 656-670, doi:10.1016/j.cell.2012.01.058 (2012).

9 Son, J. *et al.* Glutamine supports pancreatic cancer growth through a KRAS-regulated metabolic pathway. *Nature* **496**, 101, doi:10.1038/nature12040 (2013).

10 Viale, A. *et al.* Oncogene ablation-resistant pancreatic cancer cells depend on mitochondrial function. *Nature* **514**, 628-632, doi:10.1038/nature13611 (2014).

11 Santana-Codina, N. *et al.* Oncogenic KRAS supports pancreatic cancer through regulation of nucleotide synthesis. *Nat Commun* **9**, 4945, doi:10.1038/s41467-018-07472-8 (2018).

12 Humpton, T. J. *et al.* Oncogenic KRAS Induces NIX-Mediated Mitophagy to Promote Pancreatic Cancer. *Cancer Discov* **9**, 1268-1287, doi:10.1158/2159-8290.CD-18-1409 (2019).

13 Tape, C. J. *et al.* Oncogenic KRAS Regulates Tumor Cell Signaling via Stromal Reciprocation. *Cell* **165**, 910-920, doi:10.1016/j.cell.2016.03.029 (2016).

14 Storz, P. & Crawford, H. C. Carcinogenesis of Pancreatic Ductal Adenocarcinoma. *Gastroenterology*, doi:10.1053/j.gastro.2020.02.059 (2020).

15 Zhang, Y., Crawford, H. C. & Pasca di Magliano, M. Epithelial-Stromal Interactions in Pancreatic Cancer. *Annual review of physiology* **81**, 211-233, doi:10.1146/annurev-physiol-020518-114515 (2019).

16 Lyssiotis, C. A. & Kimmelman, A. C. Metabolic Interactions in the Tumor Microenvironment. *Trends in cell biology* **27**, 863-875, doi:10.1016/j.tcb.2017.06.003 (2017).

17 Cox, A. D., Fesik, S. W., Kimmelman, A. C., Luo, J. & Der, C. J. Drugging the undruggable RAS: Mission possible? *Nat Rev Drug Discov* **13**, 828-851, doi:10.1038/nrd4389 (2014).

18 Sousa, C. M. *et al.* Pancreatic stellate cells support tumour metabolism through autophagic alanine secretion. *Nature* **536**, 479-483, doi:10.1038/nature19084 (2016).

19 Zhao, H. *et al.* Tumor microenvironment derived exosomes pleiotropically modulate cancer cell metabolism. *eLife* **5**, e10250, doi:10.7554/eLife.10250 (2016).

bioRxiv preprint doi: https://doi.org/10.1101/2020.08.07.238766; this version posted August 7, 2020. The copyright holder for this preprint (which was not certified by peer review) is the author/funder, who has granted bioRxiv a license to display the preprint in perpetuity. It is made available under aCC-BY-NC-ND 4.0 International license.

20 Bertero, T. *et al.* Tumor-Stroma Mechanics Coordinate Amino Acid Availability to Sustain Tumor Growth and Malignancy. *Cell metabolism* **29**, 124-140.e110, doi:10.1016/j.cmet.2018.09.012 (2019).

21 Zhang, D. *et al.* Metabolic reprogramming of cancer-associated fibroblasts by IDH3alpha downregulation. *Cell Reports* **10**, 1335-1348, doi:10.1016/j.celrep.2015.02.006 (2015).

22 Lemons, J. M. S. *et al.* Quiescent Fibroblasts Exhibit High Metabolic Activity. *PLOS Biology* **8**, e1000514, doi:10.1371/journal.pbio.1000514 (2010).

23 Sullivan, M. R. *et al.* Quantification of microenvironmental metabolites in murine cancers reveals determinants of tumor nutrient availability. *eLife* **8**, doi:10.7554/eLife.44235 (2019).

24 Fu, A. & Danial, N. N. Grasping for aspartate in tumour metabolism. *Nature Cell Biology* **20**, 738-739, doi:10.1038/s41556-018-0137-9 (2018).

25 Gui, D. Y. *et al.* Environment Dictates Dependence on Mitochondrial Complex I for NAD+ and Aspartate Production and Determines Cancer Cell Sensitivity to Metformin. *Cell metabolism* **24**, 716-727, doi:10.1016/j.cmet.2016.09.006 (2016).

26 Sullivan, L. B. *et al.* Aspartate is an endogenous metabolic limitation for tumour growth. *Nature Cell Biology* **20**, 782-788, doi:10.1038/s41556-018-0125-0 (2018).

27 Sullivan, L. B. *et al.* Supporting Aspartate Biosynthesis Is an Essential Function of Respiration in Proliferating Cells. *Cell* **162**, 552-563, doi:10.1016/j.cell.2015.07.017 (2015).

28 Garcia-Bermudez, J. *et al.* Aspartate is a limiting metabolite for cancer cell proliferation under hypoxia and in tumours. *Nature Cell Biology* **20**, 775-781, doi:10.1038/s41556-018-0118-z (2018).

29 Alkan, H. F. *et al.* Cytosolic Aspartate Availability Determines Cell Survival When Glutamine Is Limiting. *Cell metabolism* **28**, 706-720.e706, doi:10.1016/j.cmet.2018.07.021 (2018).

30 Birsoy, K. *et al.* An Essential Role of the Mitochondrial Electron Transport Chain in Cell Proliferation Is to Enable Aspartate Synthesis. *Cell* **162**, 540-551, doi:10.1016/j.cell.2015.07.016 (2015).

31 Vasan, K., Werner, M. & Chandel, N. S. Mitochondrial Metabolism as a Target for Cancer Therapy. *Cell Metab*, doi:10.1016/j.cmet.2020.06.019 (2020).

32 Olson, K. A., Schell, J. C. & Rutter, J. Pyruvate and Metabolic Flexibility: Illuminating a Path Toward Selective Cancer Therapies. *Trends in biochemical sciences* **41**, 219-230, doi:10.1016/j.tibs.2016.01.002 (2016).

33 Hui, S. *et al.* Glucose feeds the TCA cycle via circulating lactate. *Nature* **551**, 115-118, doi:10.1038/nature24057 (2017).

34 Goodman, R. P. *et al.* Hepatic NADH reductive stress underlies common variation in metabolic traits. *Nature*, doi:10.1038/s41586-020-2337-2 (2020).

35 Titov, D. V. *et al.* Complementation of mitochondrial electron transport chain by manipulation of the NAD+/NADH ratio. *Science* **352**, 231-235, doi:10.1126/science.aad4017 (2016).

36 Molina, J. R. *et al.* An inhibitor of oxidative phosphorylation exploits cancer vulnerability. *Nature Medicine* **24**, 1036-1046, doi:10.1038/s41591-018-0052-4 (2018).

37 Halestrap, A. P. Monocarboxylic acid transport. *Compr Physiol* **3**, 1611-1643, doi:10.1002/cphy.c130008 (2013).

38 Halestrap, A. P. The monocarboxylate transporter family--Structure and functional characterization. *IUBMB Life* **64**, 1-9, doi:10.1002/iub.573 (2012).

39 Halestrap, A. P. & Wilson, M. C. The monocarboxylate transporter family—Role and regulation. *IUBMB Life* **64**, 109-119, doi:10.1002/iub.572 (2012).

bioRxiv preprint doi: https://doi.org/10.1101/2020.08.07.238766; this version posted August 7, 2020. The copyright holder for this preprint (which was not certified by peer review) is the author/funder, who has granted bioRxiv a license to display the preprint in perpetuity. It is made available under aCC-BY-NC-ND 4.0 International license.

40 Polanski, R. *et al.* Activity of the monocarboxylate transporter 1 inhibitor AZD3965 in small cell lung cancer. *Clin Cancer Res* **20**, 926-937, doi:10.1158/1078-0432.Ccr-13-2270 (2014).

41 Hong, C. S. *et al.* MCT1 Modulates Cancer Cell Pyruvate Export and Growth of Tumors that Co-express MCT1 and MCT4. *Cell Reports* **14**, 1590-1601, doi:10.1016/j.celrep.2016.01.057 (2016).

42 Sakamoto, A. *et al.* Pyruvate secreted from patient-derived cancer-associated fibroblasts supports survival of primary lymphoma cells. *Cancer Sci* **110**, 269-278, doi:10.1111/cas.13873 (2019).

43 Mick, E. *et al.* Distinct mitochondrial defects trigger the integrated stress response depending on the metabolic state of the cell. *eLife* **9**, doi:10.7554/eLife.49178 (2020).

44 Sanford-Crane, H., Abrego, J. & Sherman, M. H. Fibroblasts as Modulators of Local and Systemic Cancer Metabolism. *Cancers (Basel)* **11**, doi:10.3390/cancers11050619 (2019).

45 Schworer, S., Vardhana, S. A. & Thompson, C. B. Cancer Metabolism Drives a Stromal Regenerative Response. *Cell metabolism* **29**, 576-591, doi:10.1016/j.cmet.2019.01.015 (2019).

46 Elyada, E. *et al.* Cross-Species Single-Cell Analysis of Pancreatic Ductal Adenocarcinoma Reveals Antigen-Presenting Cancer-Associated Fibroblasts. *Cancer Discov* **9**, 1102-1123, doi:10.1158/2159-8290.CD-19-0094 (2019).

47 Ohlund, D. *et al.* Distinct populations of inflammatory fibroblasts and myofibroblasts in pancreatic cancer. *The Journal of experimental medicine* **214**, 579-596, doi:10.1084/jem.20162024 (2017).

48 Neuzillet, C. *et al.* Inter- and intra-tumoural heterogeneity in cancer-associated fibroblasts of human pancreatic ductal adenocarcinoma. *The Journal of pathology* **248**, 51-65, doi:10.1002/path.5224 (2019).

49 Hosein, A. N. *et al.* Cellular heterogeneity during mouse pancreatic ductal adenocarcinoma progression at single-cell resolution. *JCI Insight* **5**, doi:10.1172/jci.insight.129212 (2019).

50 Beloueche-Babari, M. *et al.* MCT1 Inhibitor AZD3965 Increases Mitochondrial Metabolism, Facilitating Combination Therapy and Noninvasive Magnetic Resonance Spectroscopy. *Cancer Res* **77**, 5913-5924, doi:10.1158/0008-5472.CAN-16-2686 (2017).

51 Hwang, R. F. *et al.* Cancer-associated stromal fibroblasts promote pancreatic tumor progression. *Cancer research* **68**, 918-926, doi:10.1158/0008-5472.Can-07-5714 (2008).

52 Ran, F. A. *et al.* Genome engineering using the CRISPR-Cas9 system. *Nature protocols* **8**, 2281-2308, doi:10.1038/nprot.2013.143 (2013).

53 Smith, M. C. *et al.* CXCR4 regulates growth of both primary and metastatic breast cancer. *Cancer Res* **64**, 8604-8612, doi:10.1158/0008-5472.Can-04-1844 (2004).

54 Guzman, C., Bagga, M., Kaur, A., Westermarck, J. & Abankwa, D. ColonyArea: an ImageJ plugin to automatically quantify colony formation in clonogenic assays. *PloS one* **9**, e92444, doi:10.1371/journal.pone.0092444 (2014).

bioRxiv preprint doi: https://doi.org/10.1101/2020.08.07.238766; this version posted August 7, 2020. The copyright holder for this preprint (which was not certified by peer review) is the author/funder, who has granted bioRxiv a license to display the preprint in perpetuity. It is made available under aCC-BY-NC-ND 4.0 International license.

EXTENDED DATA FIGURES

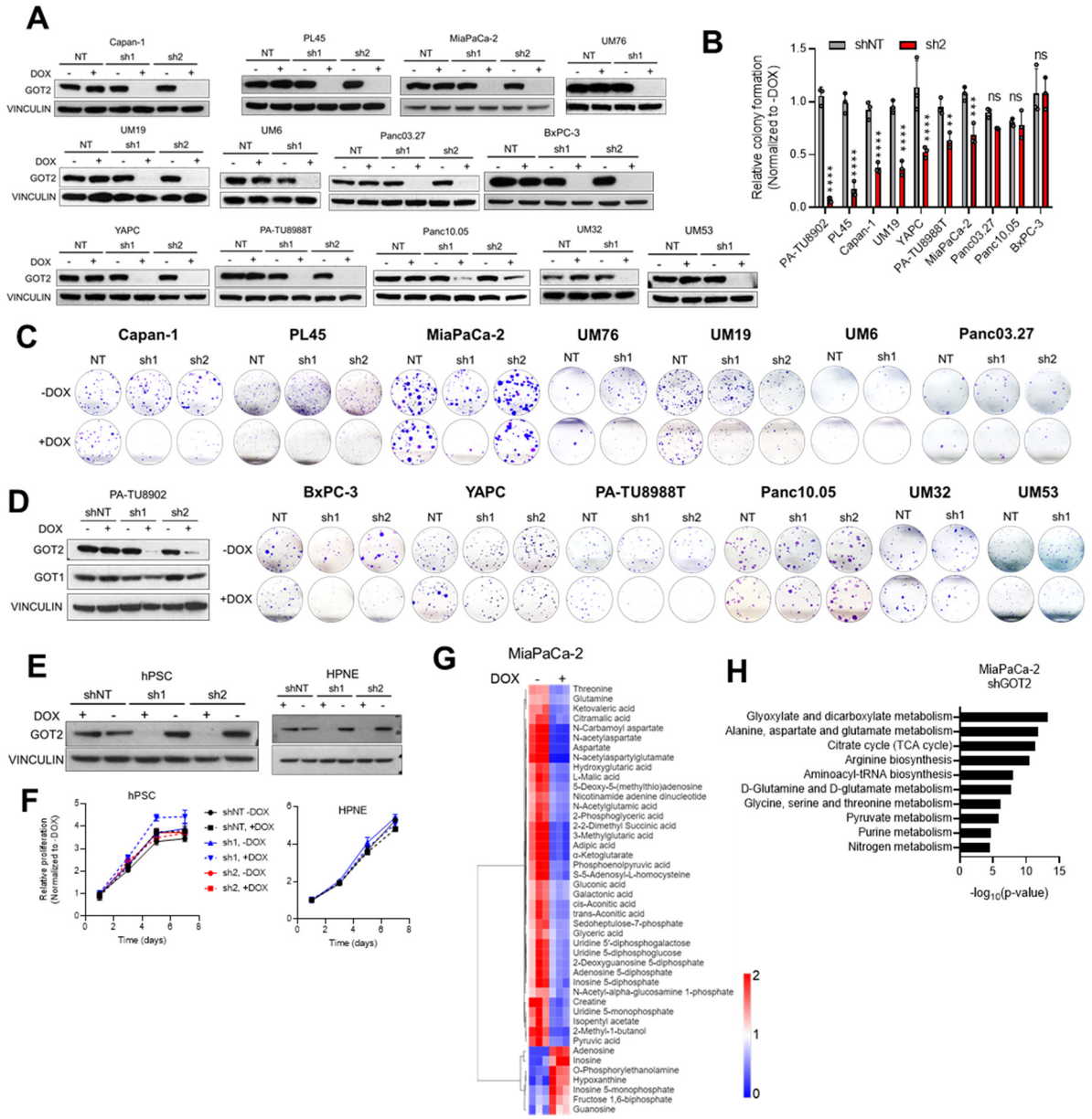

Extended Data Fig.1 A) Western blots of GOT2 expression with Vinculin loading control in PDA cells expressing doxycycline-inducible shNT or two independent shRNA sequences against GOT2. **B)** Relative colony formation after GOT2 knockdown with sh2 across a panel of PDA cell lines. **C)** Images of representative wells showing PDA colony formation after GOT2 knockdown. **D)** Western blot for GOT1 and GOT2 with Vinculin loading control in PA-TU8902 cells after GOT2 knockdown. **E)** Western blots of GOT2 expression with Vinculin loading control in HPNE or hPSC cell lines expressing doxycycline-inducible shNT or two independent shRNA sequences against GOT2. **F)** Relative proliferation of HPNE or hPSC cell lines after GOT2 knockdown. **G,H)** Metabolites significantly changed between +DOX (n=3) and –DOX (n=3) ($p<0.05$, $-1>\log2FC>1$) in MiaPaCa-2 GOT2 knockdown cells as assessed by metabolomics. **G)** Heatmap depicting changes in relative metabolite abundances with 2D unsupervised hierarchical clustering. **H)** Metabolic pathways significantly changed in MiaPaCa-2 cells, as determined via Metaboanalyst. Bars represent mean ± SD, *$p<0.05$, **$p<0.01$, ***$p<0.001$, ****$p<0.0001$.

bioRxiv preprint doi: https://doi.org/10.1101/2020.08.07.238766; this version posted August 7, 2020. The copyright holder for this preprint (which was not certified by peer review) is the author/funder, who has granted bioRxiv a license to display the preprint in perpetuity. It is made available under aCC-BY-NC-ND 4.0 International license.

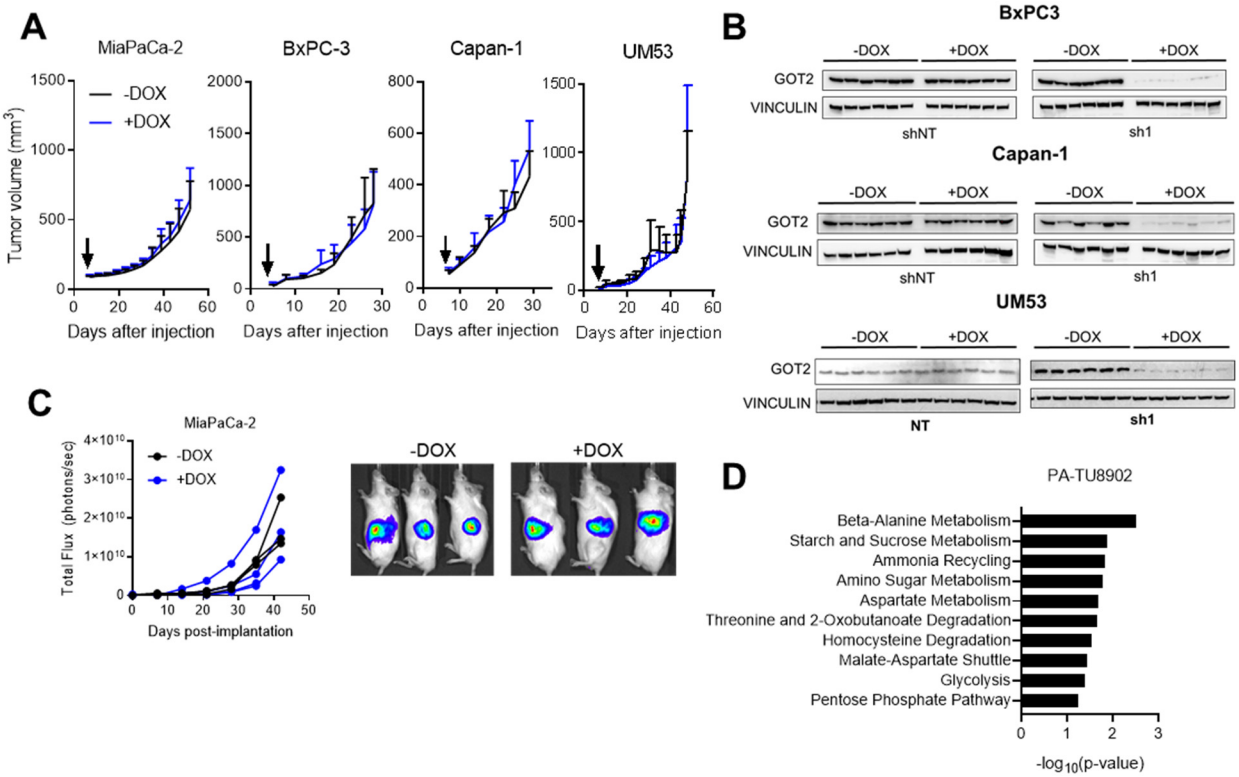

Extended Data Fig.2 A) Growth across a panel of subcutaneous PDA control shNT tumors in NSG mice (n=6 tumors per group). Arrows indicate administration of doxycycline chow. **B)** Western blot for expression of GOT2 and Vinculin loading control in PDA GOT2 knockdown subcutaneous tumors. **C)** Radiance of MiaPaCa-2 GOT2 knockdown orthotopic tumors in NSG mice, with bioluminescent images at endpoint. **D)** Metabolic pathways significantly changed between +DOX (n=6) and –DOX (n=6) ($p<0.05$, $-0.5>\log2FC>0.5$) in PA-TU8902 GOT2 knockdown subcutaneous tumors, as determined via Metaboanalyst. Bars represent mean ± SD, *$p<0.05$, **$p<0.01$, ***$p<0.001$, ****$p<0.0001$.

bioRxiv preprint doi: https://doi.org/10.1101/2020.08.07.238766; this version posted August 7, 2020. The copyright holder for this preprint (which was not certified by peer review) is the author/funder, who has granted bioRxiv a license to display the preprint in perpetuity. It is made available under aCC-BY-NC-ND 4.0 International license.

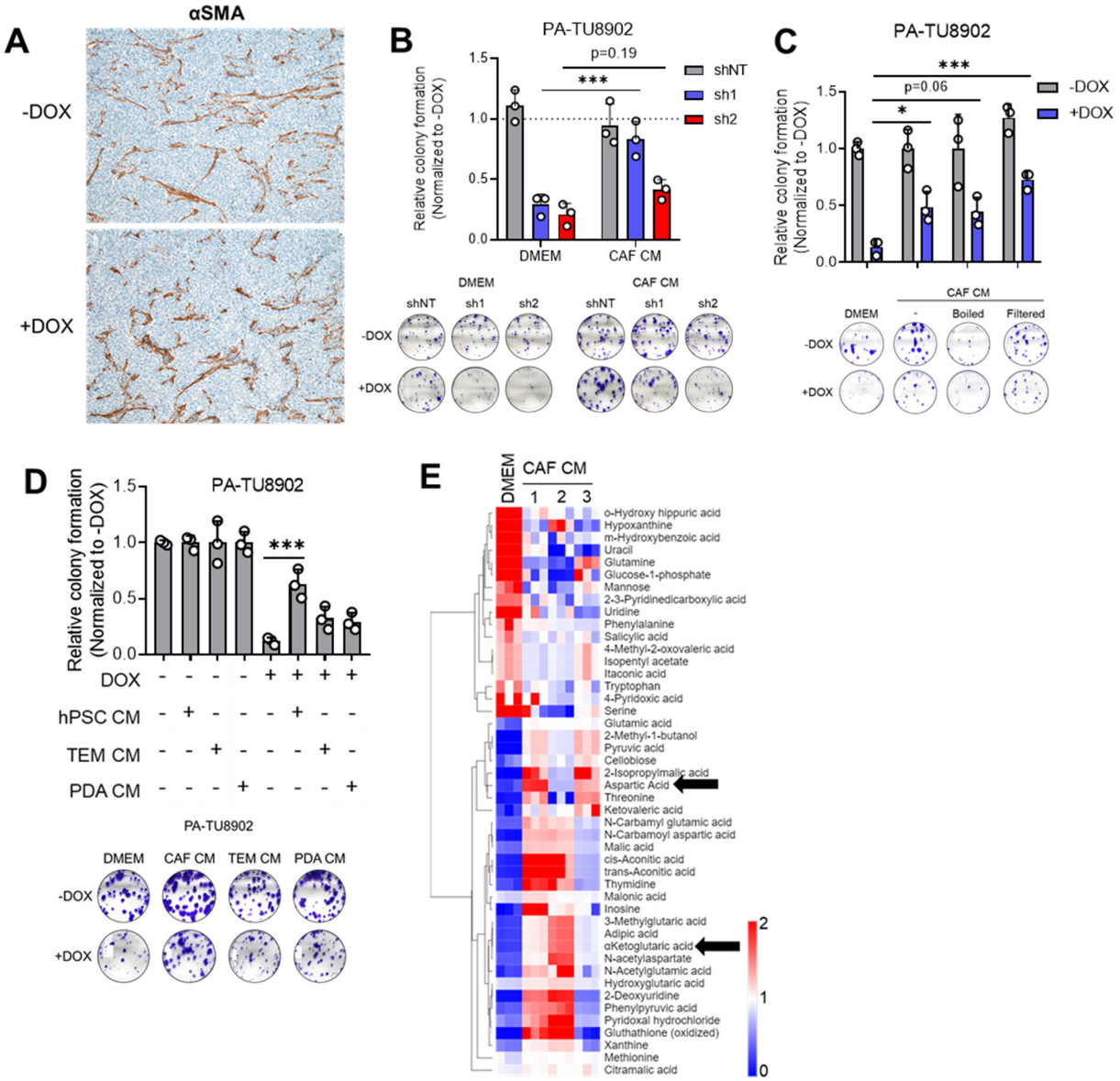

Extended Data Fig.3 A) Representative αSMA staining in tissue slices from PA-TU8902 subcutaneous tumors from Fig.2A. **B)** Relative colony formation of PA-TU8902 GOT2 knockdown cells cultured in DMEM or CAF CM, with images of representative wells. **C)** Relative colony formation of PA-TU8902 GOT2 knockdown cells cultured in DMEM or fresh CAF CM, boiled CM, CM passed through a 3 kD filter, or CM subjected to freeze/thaw cycles, with images of representative wells. **D)** Relative abundances of metabolites significantly ($p<0.05$) changed between CAF CM and DMEM, as determined by metabolomics. Asp and αKG are indicated with black arrows. **E)** Relative colony formation of PA-TU8902 GOT2 knockdown cells cultured in DMEM or CAF CM, tumor educated macrophage (TEM) CM, or PA-TU8902 CM. Bars represent mean ± SD, *$p<0.05$, **$p<0.01$, ***$p<0.001$, ****$p<0.0001$.

bioRxiv preprint doi: https://doi.org/10.1101/2020.08.07.238766; this version posted August 7, 2020. The copyright holder for this preprint (which was not certified by peer review) is the author/funder, who has granted bioRxiv a license to display the preprint in perpetuity. It is made available under aCC-BY-NC-ND 4.0 International license.

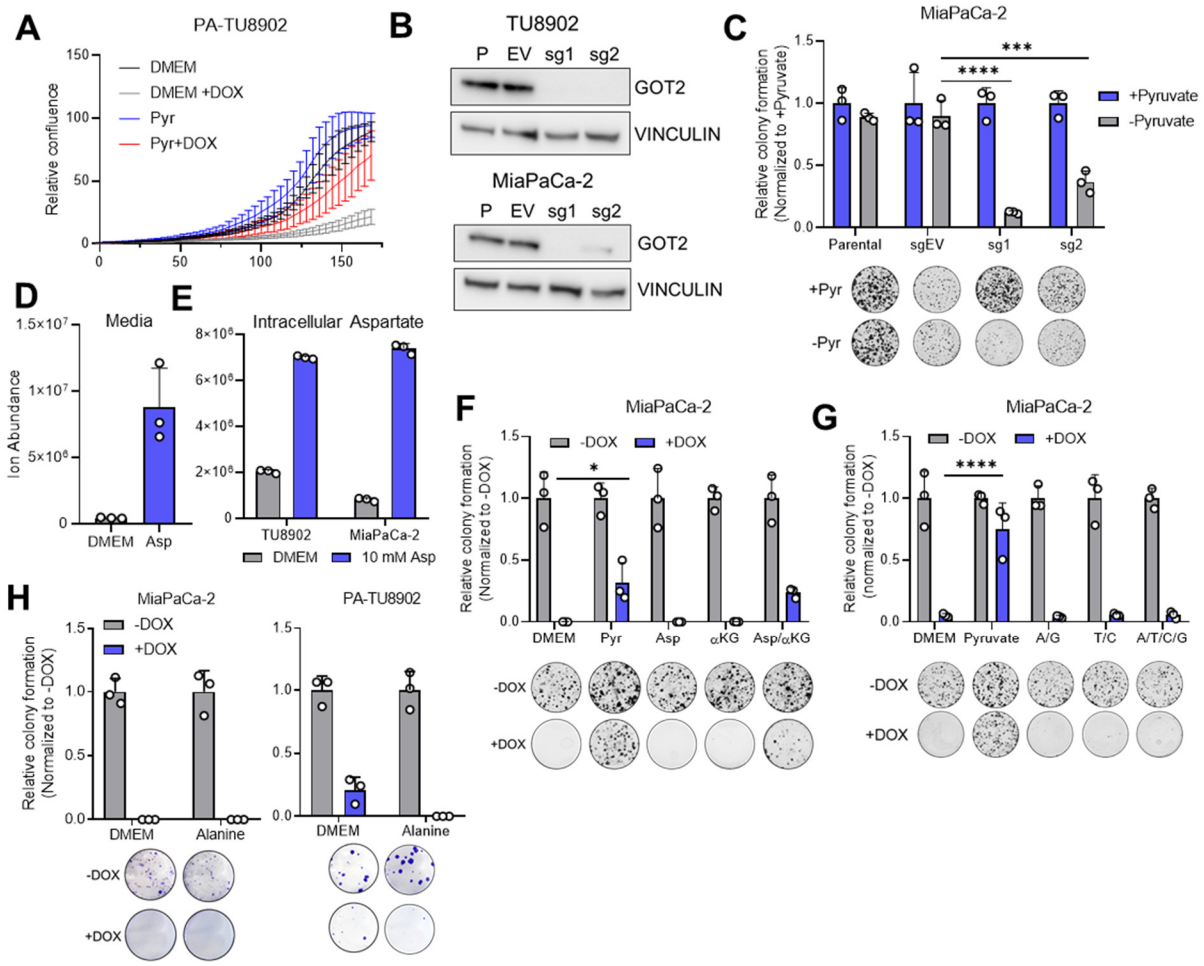

Extended Data Fig.4 A) Relative confluence over time of PA-TU8902 GOT2 knockdown cells cultured in DMEM or 1 mM pyruvate. **B)** Western blot for GOT2 expression in parental PA-TU8902 and MiaPaCa-2 cells, or cells transfected with an empty vector or two independent single guide (sg)GOT2 sequences, with Vinculin loading control. **C)** Relative colony formation of MiaPaCa-2 GOT2 knockout cells cultured in DMEM or 1 mM pyruvate, with images of representative wells. **D)** Relative abundance of aspartate in DMEM or media containing 10 mM aspartate, as measured by LC/MS. **E)** Relative abundance of aspartate in PA-TU8902 or MiaPaCa-2 cells after culture in DMEM or 10 mM aspartate, as measured by LC/MS. **F)** Relative colony formation of MiaPaCa-2 GOT2 knockdown cells cultured in DMEM, 10 mM aspartate, 4 mM αKG, or both Asp/αKG, with images of representative wells. **G)** Relative colony formation of MiaPaCa-2 GOT2 knockdown cells cultured in DMEM or 100 μM of the indicated combinations of adenine (A), guanine (G), thymine (T), and cytosine (C), with images of representative wells. **H)** Relative colony formation of MiaPaCa-2 or PA-TU8902 GOT2 knockdown cells cultured in DMEM or 1 mM alanine, with images of representative wells. Bars represent mean ± SD, *p<0.05, **p<0.01, ***p<0.001, ****p<0.0001.

bioRxiv preprint doi: https://doi.org/10.1101/2020.08.07.238766; this version posted August 7, 2020. The copyright holder for this preprint (which was not certified by peer review) is the author/funder, who has granted bioRxiv a license to display the preprint in perpetuity. It is made available under aCC-BY-NC-ND 4.0 International license.

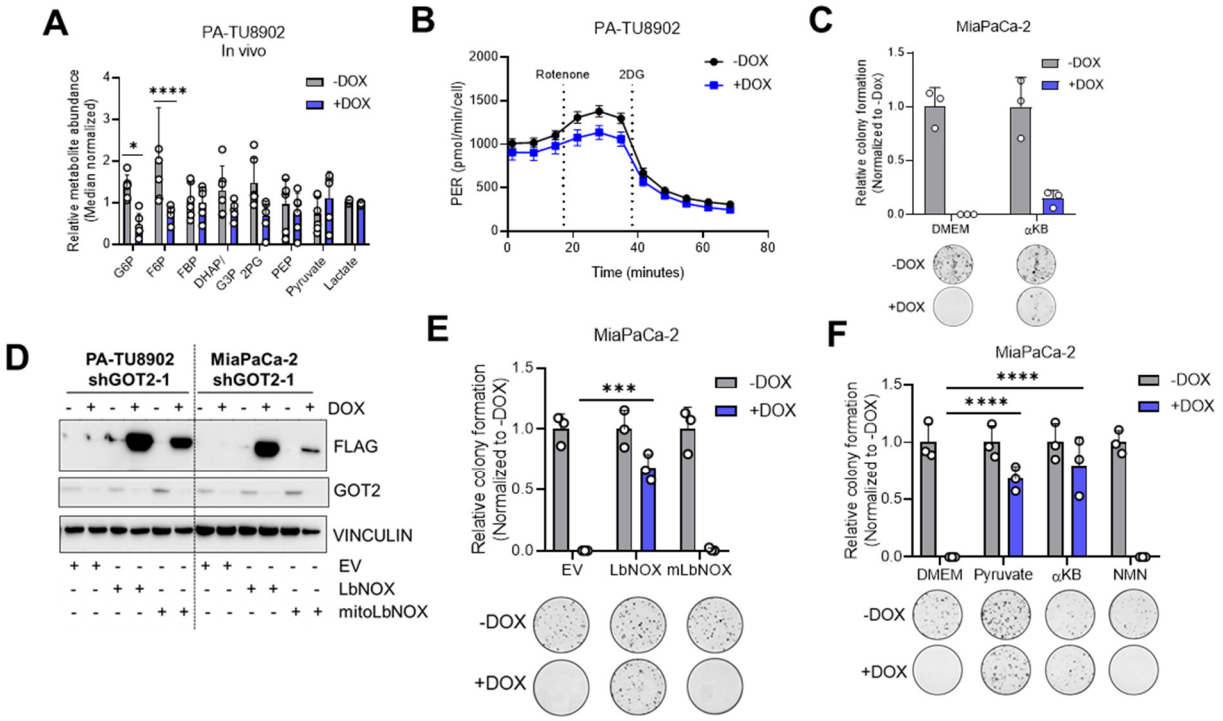

Extended Data Fig.5 A) Relative abundances of glycolytic intermediates in PA-TU8902 GOT2 knockdown subcutaneous tumors. **B)** Proton efflux rate (PER) of PA-TU8902 GOT2 knockdown cells cultured +DOX for 3 days, as determined by the Glycolytic Rate Assay. **C)** Relative colony formation of MiaPaCa-2 GOT2 knockdown cells cultured in DMEM or 1 mM αKB, with images of representative wells. **D)** Western blot for Flag-tagged, doxycycline-inducible LbNOX or GOT2, with Vinculin loading control, in PA-TU8902 or MiaPaCa-2 GOT2 knockdown cells. **E)** Relative colony formation of MiaPaCa-2 GOT2 knockdown cells expressing cytosolic or mitochondrial LbNOX. **F)** Relative colony formation of MiaPaCa-2 GOT2 knockdown cells cultured in DMEM, 1 mM pyruvate, αKB, or NMN, with images of representative wells. Bars represent mean ± SD, *p<0.05, **p<0.01, ***p<0.001, ****p<0.0001.

bioRxiv preprint doi: https://doi.org/10.1101/2020.08.07.238766; this version posted August 7, 2020. The copyright holder for this preprint (which was not certified by peer review) is the author/funder, who has granted bioRxiv a license to display the preprint in perpetuity. It is made available under aCC-BY-NC-ND 4.0 International license.

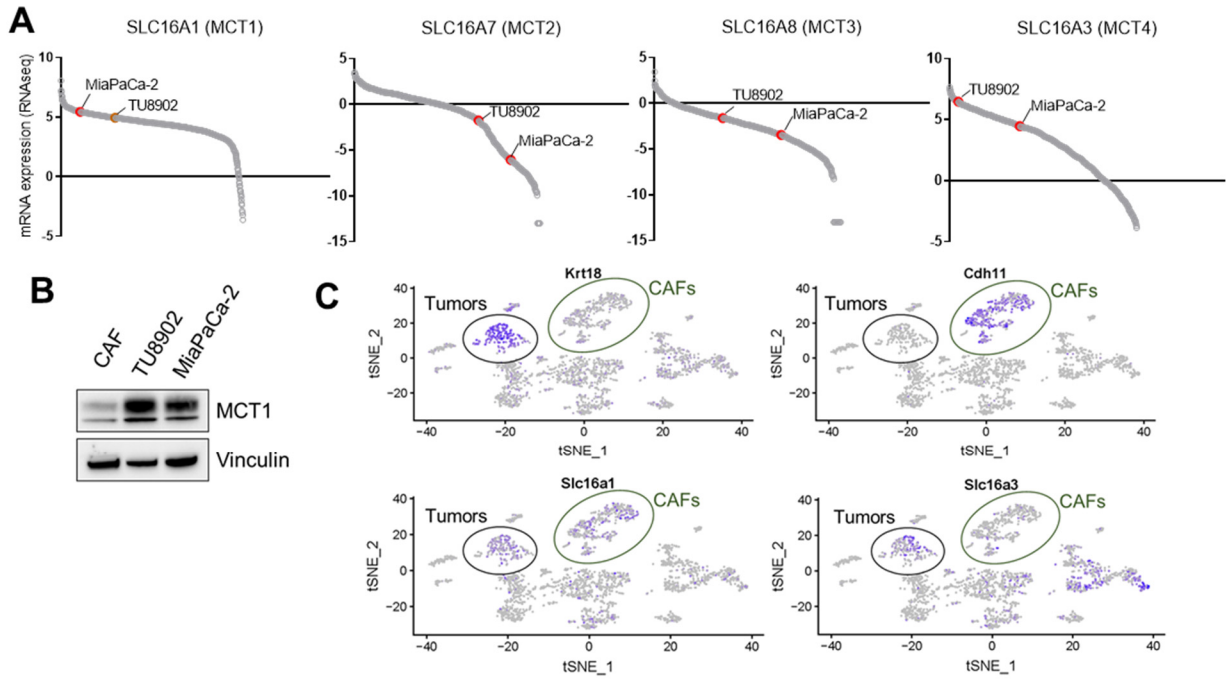

Extended Data Fig.6 A) CCLE relative transcript expression levels of MCT family members in PDA cell lines. **B)** Western blot for MCT1, with vinculin loading control, in CAFs or PA-TU8902 and MiaPaCa-2 cells. **C)** Single-cell RNA sequencing data from KPC syngeneic orthotopic tumors showing expression of Slc16a1 (MCT1) and Slc16a3 (MCT4) in CAF (CDH11) and epithelial (Krt18) populations.